國立臺灣大學電機資訊學院光電工程學研究所

碩士論文

Graduate Institute of Photonics and Optoelectronics

College of Electrical Engineering and Computer Science

National Taiwan University

Master's Thesis

電位影像螢光光子統計之模擬研究

A Simulation Study on Fluorescence Photon Statistics of Voltage Imaging

黃書安

Shu-An Hwang

指導教授 ： 孫啟光 博士

Advisor: Chi-Kuang Sun, Ph.D.

中華民國 114 年 6 月

June 2025

doi:10.6342/NTU202501717

誌謝

這一篇論文的完成過程當中，充滿了挑戰與種種困難，然而能夠引領我走到這一步的，絕對不僅僅是我自己的功勞。我必須誠摯感謝我的指導教授、合作的教授、合作對象的學生或助理、實驗室的同學與學長學弟，所有一路以來任何在研究方面協助過我的人，是他們讓我能夠完成這份研究。

首先當然必須要感謝我的指導教授孫啟光老師，在這份研究上給予了我不論是從大方向，或是到小細節，各方面的專業指導。老師即使總是十分忙碌，在我需要跟老師討論研究事項的時候還是會非常認真地參與並提供專業意見。

另外要感謝合作對象陳示國教授，以及他們實驗室的廖柏澤同學，在電位影像實驗的部分給予我許多相關幫助及專業建議。還有李妮鐘醫師，以及她的研究助理 Andy，在我的實驗小鼠準備方面提供了全方位的協助，所有的樣品製備都是由他完成，可以說是我論文中實驗相關數據能夠完成，最不可或缺的角色。

最後還要感謝我們實驗室的，耀暐學長，不厭其煩的幫我載各種實驗樣品。彭瑞學長，在實驗或理論知識方面都不吝於提供他的幫忙及相關建議。冠穎學長，教會我實驗室的各種知識及實驗上的幫助。昱鑫學弟，在電位影像實驗方面提供了許多幫助及建議。

我要在這邊向以上這些人，所有給予我幫助或鼓勵的同學，抑或是我的家人致上最高的謝意。有了他們，才能讓我走到今天這一步，完成這篇碩士論文。

doi:10.6342/NTU202501717

摘要

本研究的重點在於從光子統計的角度出發，創造一個關於雙光子電位影像的模擬方法。由於目前在雙光子電位影像的領域當中，其影像礙於散粒雜訊的限制下，以至於電位影像的亮度成為一項至關重要的議題。本研究也曾致力於做小鼠中腦黑質致密部（ＳＮｃ）的電位影像研究，然而同樣受限於平均光子數不足，以至於無法看到明顯電位變化。因此，我們從光子統計的角度出發，設計了一套模擬方法，去研究電位影像中的電信號被偵測的可能性。

在本研究的模擬當中，假設了一套完美的量測系統，將重心放在光子數的統計行為上面。以此證明，假若在完美量測系統的條件下，模擬出無法偵測到螢光變化，那麼真實情況便更不可能足以達到可偵測電位訊號的條件。

本研究的模擬方法，提供了相關電位影像實驗的設計去做電位信號評估。依照本研究總結出的幾個重要相關參數，可以評估參數下的實驗條件，其電位信號被偵測的靈敏度及準確率。

關鍵字：雙光子顯微鏡、光子統計、電位影像

doi:10.6342/NTU202501717

ABATRACT

The point of this study was to create a two-photon voltage imaging simulation from the perspective of photon statistics. In the field of two-photon voltage imaging, the quality of the images is often limited by shot noise, making brightness a critical issue for the detectability of voltage signals. Our research initially involved in vivo experiments using the ASAP4e GEVIs in the substantia nigra pars compacta (SNc) of the mice brain. However, the experiments were limited by low photon counts, which prevented the detection of clear voltage signals. Thus, from the perspective of photon statistics we designed a simulation method, to investigate the possibility of spike detection in voltage imaging.

In the simulation of this study, a perfect measurement system was assumed, focusing on the photon statistical behavior. This is to demonstrate that if voltage signal spikes cannot be detected even under ideal conditions, their detection under real experimental conditions would be impossible.

This thesis has provided a simulation method to relevant voltage imaging experiments, assessing the voltage signal quality. Based on some important parameters in the summary of this thesis, it is able to evaluate the spike detection sensitivity and precision under the experimental parameters.

doi:10.6342/NTU202501717

Keywords: Two-photon microscopy, Photon statistics, Voltage imaging

doi:10.6342/NTU202501717

CONTENT

doi:10.6342/NTU202501717

doi:10.6342/NTU202501717

doi:10.6342/NTU202501717

FIGURES

doi:10.6342/NTU202501717

doi:10.6342/NTU202501717

doi:10.6342/NTU202501717

doi:10.6342/NTU202501717

TABLE

doi:10.6342/NTU202501717

Chapter 1 Introduction

1.1 Motivation

Recently, numerous studies have focused on Genetically Encoded Voltage Indicators (GEVIs) and their applications in in vivo imaging, they have also proved the advantages of GEVIs over Genetically Encoded Calcium Indicators (GECIs). Inspired by these researches, we sought to develop an in vivo experimental system using the GEVI ASAP4 to record voltage activity in the mouse substantia nigra pars compacta (Sc).

Although the original experimental goal was not successfully achieved, the study led to the identification of an alternative yet important question: from the perspective of evaluating the photon statistical behavior of voltage imaging photon emission rate, how voltage spike signals perform and how their detectability is affected by severe shot noise. The shot noise issue is a major bottleneck in two-photon imaging using GEVIs.

The aims of this study are therefore twofold:

1. Assessing the photon emission rate of voltage imaging under two-photon excitation based on our in vivo experimental data

2. Establishing a simulation framework to evaluate the sensitivity and precision of

doi:10.6342/NTU202501717

voltage signal detection under various experimental conditions.

1.2 Thesis Scope

In this thesis, Chapter 2 will give some background knowledge of this study. Including the principles of two-photon microscopy, brief introduction to the photodetectors and photon statistics, the Genetically Encoded Voltage Indicators (GEVIs).

Chapter 3 will show some experiments about voltage imaging, it can be separated into two parts. First, we'll give some examples of the previous studies about the voltage imaging experiment. Then, we'll get into the part of the in vivo voltage imaging experiment done by ourselves.

Chapter 4 will get into the most important part, the simulation method. In this chapter we will describe the details and the method of our simulation, and how we built the simulation model. We're also going to introduce some important parameters of the simulation.

Chapter 5 then shows the results of our simulation. Including the results from different variables. We've analyzed some theoretical trend of the result. Some extended results will also be shown.

Chapter 6 summarizes the thesis and talks about some possible future works

doi:10.6342/NTU202501717

extended from this study.

doi:10.6342/NTU202501717

CHAPTER 2 BACKGROUND KNOWLEDGE

2.1 Principles of Two-Photon Microscopy

Two-Photon Fluorescence Microscopy (2PFM) is a kind of nonlinear microscopy, whose concept principle is established on the capability of absorbing two low-energy photons by a single fluorescence molecule in a very short time. Different with the conventional single-photon absorption, the two-photon emission depends on high-power pulsed laser, such as femtosecond pulsed laser, who has the ability to form up enough photon density on the focal point, letting the molecules simultaneously absorb two infrared photons in nonlinear third-order probability, excited to the fluorescent state, then returns to the ground state [1].

There are several key advantages of this technology. First, it substantially reduces photobleaching and photodamage outside the focal point. Second, with near-infrared excitation light, it has the ability to penetrate the deeper biological tissue, while maintaining high spatial resolution. These advantages make two-photon microscopy widely applicable in neuroscience [2].

2.2 Photodetectors and Photon statistics

In the context of two-photon fluorescence microscopy, detecting weak fluorescence signals emitted from deep tissue using sensitive photodetectors has become an

doi:10.6342/NTU202501717

important issue. Among plenty types of photodetectors, the photomultiplier tube (PMT) became a widely used option due to its high gain and fast response time [3].

Photomultiplier tube (PMT) operates by amplifying a single incident photon into a measurable electrical pulse through a photocathode, a series of dynodes and an anode, achieving gains on the order of about 10^6 to 10^7 [4].

In low-light two-photon fluorescence imaging, besides using the high-gain photomultiplier tubes (PMTs) as the photon detector, the photon-level statistical behavior of fluorescence molecule emission is also a critical issue. In the subsequent section, we will evaluate the average photon number under two-photon excitation conditions, show the photon-level brightness of the acquired images.

Lots of research groups have done the investigations of photon statistics in single-molecule fluorescence emission [5-7]. The results showed that single-molecule fluorescence can exhibit **sub-Poisson** statistics at short time intervals, caused by photon antibunching resulting from ground state recovery delay. Conversely, at longer time intervals, the presence of triplet state relaxation introduces photon bunching, leading to **super-Poisson** statistics [5]. However, the studies also showed that under multi-molecule condition, the photon statistics tend to display classical **Poisson** behavior rather than sub-Poisson [8]**.** Moreover, the duration of the excitation pulse relative to the

doi:10.6342/NTU202501717

fluorophore's lifetime further determines whether bunching or antibunching can be observed. When the excitation interval (e.g., 12.5 ns in our experimental condition) exceeds the fluorescence lifetime (~2.5 ns for GFP), the molecule returns to the ground state well before the next excitation event. The study demonstrated that when inter-pulse delays exceed the fluorescence lifetime, photon statistics transfer into classical Poisson statistics [9].

Therefore, under the experimental and simulation conditions with multiple fluorescent molecules and excitation periods longer than the fluorescence lifetime, it is valid to model photon emission as a Poisson process.

Given the above considerations, the Poisson distribution provides a suitable statistical model for describing the number of photon detection events occurring within an interval time. The probability of observing k photon events during a given interval can be described by the Poisson probability mass function [10]:

$$P(k;\lambda) = \frac{\lambda^k e^{-\lambda}}{k!} \qquad (2.1)$$

Where k is the number of observed photon-counts, and λ is the expected number (mean photon rate) in the given interval.

In the context of two-photon microscopy voltage imaging, this framework provides an efficient and reasonable method for our simulation of the fluorescence photon

doi:10.6342/NTU202501717

emission model, as will be discussed for more details in Chapter 4.

2.3 Genetically Encoded Voltage Indicators (GEVIs)

Genetically encoded voltage indicators (GEVIs) is a fluorescent protein-based sensor, who has the ability to directly report the fluorescent change induced by the membrane potential change. Genetically encoded voltage indicators (GEVIs) combine the Voltage-Sensing Domain (VSD) with fluorescent protein, so when the membrane potential change, the fluorescent protein conformational change to induce the fluorescent signal [11]. The application of GEVIs has significantly promoted various kinds of neuroscience studies of in vivo systems, including mouse cortex, zebrafish, and Drosophila brain preparations [12].Compared to Genetically Encoded Calcium Indicators (GECIs), the key advantage of GEVIs would be the high temporal resolution and potential tracking precision.

doi:10.6342/NTU202501717

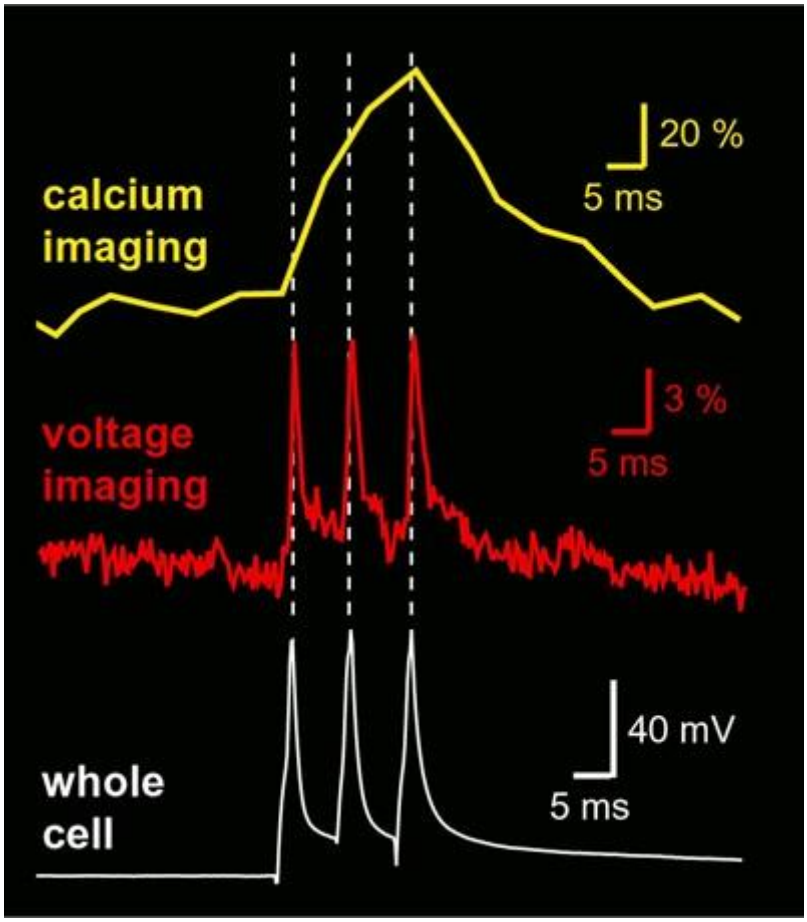

Fig. 2.1 The temporal resolution comparison between Genetically Encoded Calcium Indicators (GECIs) and Genetically Encoded Voltage Indicators (GEVIs) [13].

In our study, for some of the in vivo experiments in the next chapter, we adopted the ASAP4e GEVIs, which is a positive tuned voltage indicator. Compared to the previous generation of their ASAP family, the ΔF/F has also been promoted [14], where F was defined as the fluorescence intensity.

doi:10.6342/NTU202501717

CHAPTER 3 IN VIVO MICE EXPERIMENT

3.1 Previous Studies on Two-Photon GEVIs Imaging

There have been many research groups devoted efforts to neuroscience studies using Genetically Encoded Voltage Indicators (GEVIs). Meanwhile, demonstrating their advantages over Genetically Encoded Calcium Indicators (GECIs). Next, we're going to show some representative studies involving GEVIs experiments.

3.1.1 ASAP4 GEVI

First, we want to introduce a great development of Genetically Encoded Voltage Indicators (GEVIs), ASAP4, which is the fourth-generation sensor of their ASAP family. We have also adopted this GEVI for our in vivo mice experiments.

Unlike their earlier version, ASAP4 is a positively tuned GEVI, meaning the fluorescent change increase during depolarization. It exhibits greater photostability, higher fluorescence baseline and better ΔF/F.

In their study published in 2023 [14], Evans et al. have done lots of experiments of ASAP4, such as both in vivo one-photon and two-photon imaging on various regions of the mouse brain, including hippocampus and motor cortex.

Most notably, they simultaneously expressed ASAP4e (GEVI) and jRGECO1 (GECI) in the mouse visual cortex, allowing dual-color two-photon imaging. Fig. 3.1

doi:10.6342/NTU202501717

has shown the result. It shows that ASAP4e provided higher temporal resolution than jRGECO1a. Also, it captured the voltage faster than calcium imaging.

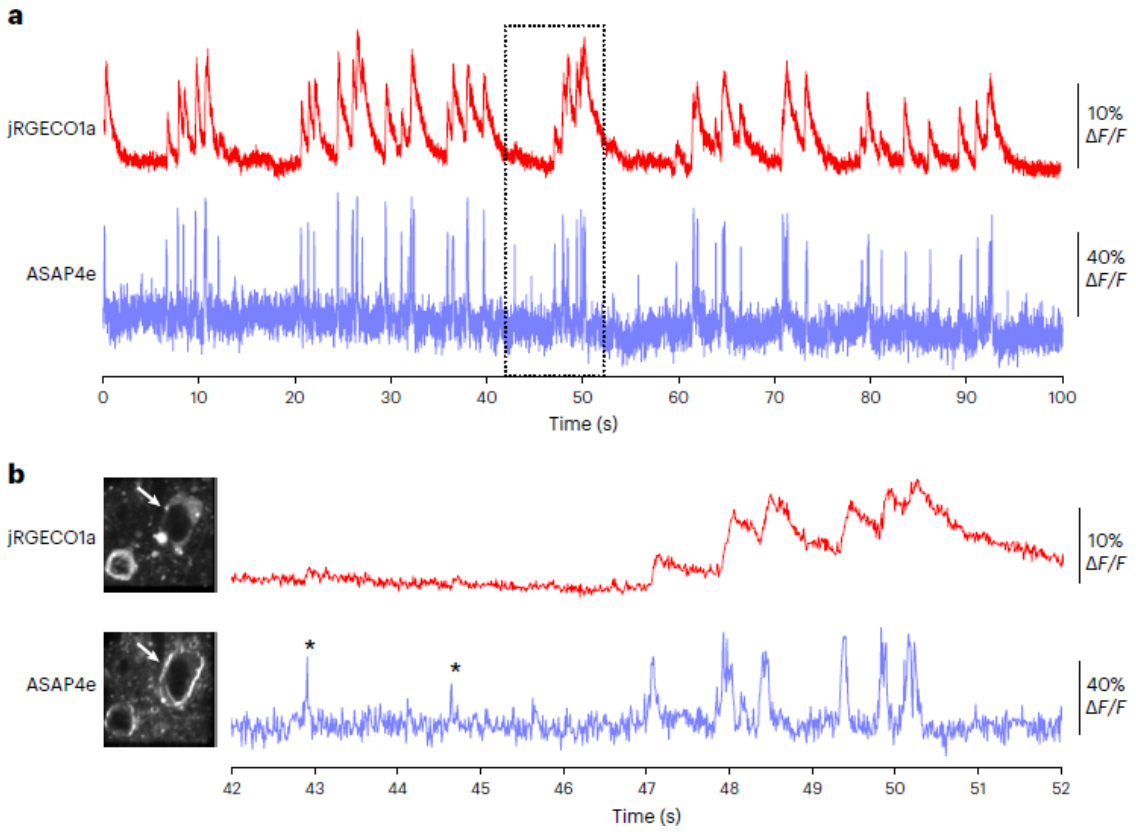

Fig. 3.1 Simultaneous ASAP4e (GEVI) and jRGECO1a (GECI) imaging in the mouse visual cortex.

Here we make some comparison of their photon emission rate with our experimental data in 3.2. They didn't provide enough experimental setting, such as PMT gain and DAQ voltage input range to calculate the photon rate like we will do in 4.2.2, so let's estimate the photon emission rate from some known conditions. For the photon

doi:10.6342/NTU202501717

number absorbed per fluorophore per pulse, it has been shown in the study [1]

$$n_a = \frac{{p_0}^2 \delta}{\tau_p {f_p}^2} \left(\frac{A^2}{2\hbar c \lambda}\right)^2 \quad (3.1)$$

Where A is the numerical aperture, p_0 is the average laser power, u_p is the laser repetition rate. Assume other parameters to be the same the relation of n_{ab} would be

$$n_a \propto \frac{{p_0}^2 A^4}{{f_p}^2} \quad (3.2)$$

Then for the emission photon number in the whole area, and assume the fluorophore quantum efficiency to be the same, the total emission photon number per pulse would be

$$n_e \propto \frac{{p_0}^2 A^2}{{f_p}^2} \quad (3.3)$$

Table 3.1 shows these relevant parameters between our experiment

Table 3.1 Some experimental parameters in ASAP4 article and our in vivo experiment.

	ASAP4 article	This thesis
Average Power (p_0)	30 (mw)	45 (mw)
Numerical Aperture (A)	0.8	0.45
Repetition Rate (f_p)	80 (MHz)	80 (MHz)

From Eq. (3.3), the relationship between their emission photon number per pulse n_{e1} and

doi:10.6342/NTU202501717

our emission photon number per pulse n_{e0} would be

$$\frac{n_{e1}}{n_{e0}} = \left(\frac{30}{45}\right)^2 \left(\frac{0.8}{0.45}\right)^2 = 1.4 \quad (3.4)$$

However, in the subsequent section, we'll show that the ROI pixel number is also an important parameter to affect the spike detection sensitivity. In this ASAP4 article, they had provided their raw image data, it showed that their ROI pixel number was about 3796 pixels, which is more than twice as many as ours.

3.1.2 Spikey Gi and SpikeyGi2 GEVI

There is another notable application of GEVI two-photon imaging study we want to introduce. They have developed two positively tuned GEVIs, spikey and SpikeyGi2, and performed the in vivo large scale neuronal voltage imaging with SMURF two-photon microscope built by themselves [15].

In the study, they expressed spikey Gi and SpikeyGi2 in the primary somatosensory cortex (S1), using air-puff stimulation to conduct the sensory-evoked voltage response. Fig. 3.2 has showed some results of the performance of their spikey Gi and SpikeyGi2 in vivo experiment. It shows that compared to ASAP3, spikey and SpikeyGi2 showed higher peak response. Also, the traces showed great isolated spike responses for each air puff.

doi:10.6342/NTU202501717

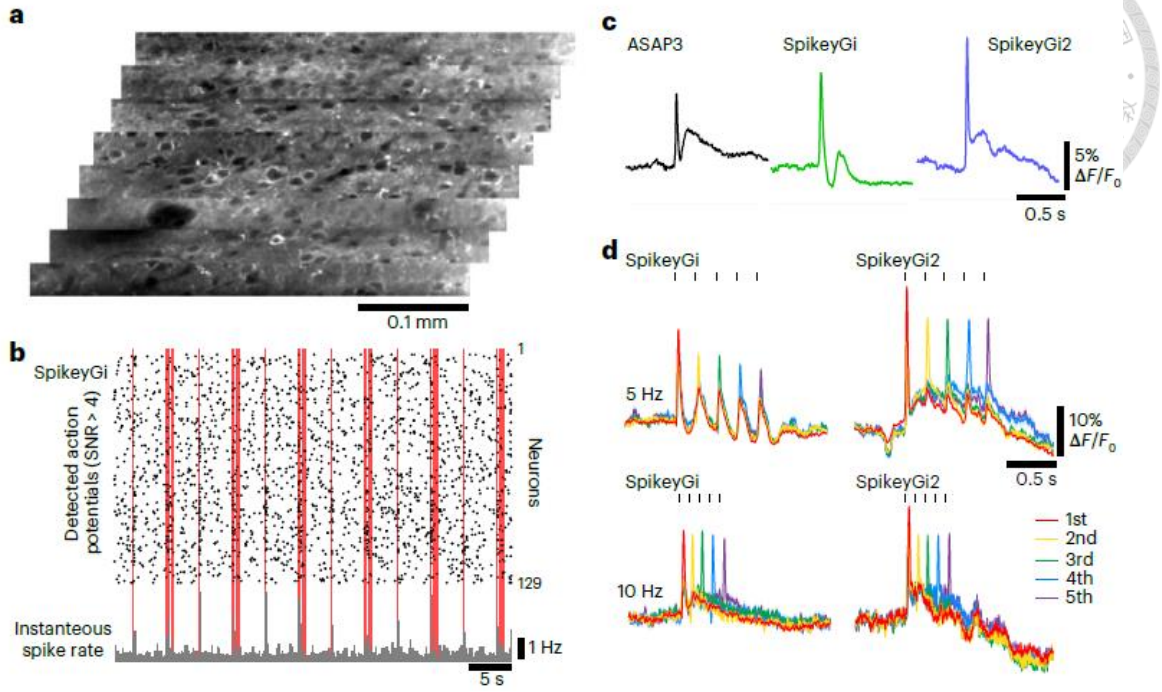

Fig. 3.2 In vivo two-photon imaging of spikey Gi and SpikeyGi2 in the primary somatosensory cortex (S1).

Like we did in 3.1.1, Table 3.1 shows some parameters between our experiments

Table 3.2 Some experimental parameters in spikey article and our in vivo experiment.

	spikey Gi article	This thesis
Average Power (p_0)	30 (mw)	45 (mw)
Numerical Aperture (A)	0.8	0.45
Repetition Rate (f_p)	31.25 (MHz)	80 (MHz)

From Eq. (3.3), the relationship between their emission photon number per pulse n_{e2} and

doi:10.6342/NTU202501717

our emission photon number per pulse n_{e0} would be

$$\frac{n_{e2}}{n_{e0}} = \left(\frac{30}{45}\right)^2 \left(\frac{0.8}{0.45}\right)^2 \left(\frac{80}{31.25}\right)^2 = 9.24 \quad (3.5)$$

For the ROI pixel number of the spikey article, they didn't provide their raw image data, so we could not estimate their ROI pixel number. However, their SMURF two-photon microscope allowed them to increase scanning pixel number under 803-Hz frame rate with the multiplexing method, the detail of their microscope design has been shown in the article.

3.1.3 Two-photon voltage imaging with adaptive excitation

Another research about voltage imaging was published by Zhao et al [16], who have developed the adaptive excitation source (AES) system. The system utilizes a Pockels cell driven by arbitrary waveform generator (AWG) to selectively deliver high-frequency laser pulses only within regions of interest (ROIs). Through this method, they were able to enhance the fluorescence signal in the region of interest (ROI) without increasing the average laser power.

Fig. 3.3 has shown their in vivo voltage imaging results in the mouse visual cortex, in which neurons expressed the genetically encoded voltage indicator ASAP5. It shows that under the same average laser power, the AES system achieved a significantly improved signal-to-noise ratio (SNR) compared to conventional uniform scanning.

doi:10.6342/NTU202501717

Notably, they have provided the quantified average photon number per neuron per frame. In Fig. 3.3, it shows that after using AES, the ROI photon number has increased from 16 to 740. In the last chapter of this thesis, we'll also demonstrate that such a difference in photon number can lead to a substantial improvement in spike detection performance.

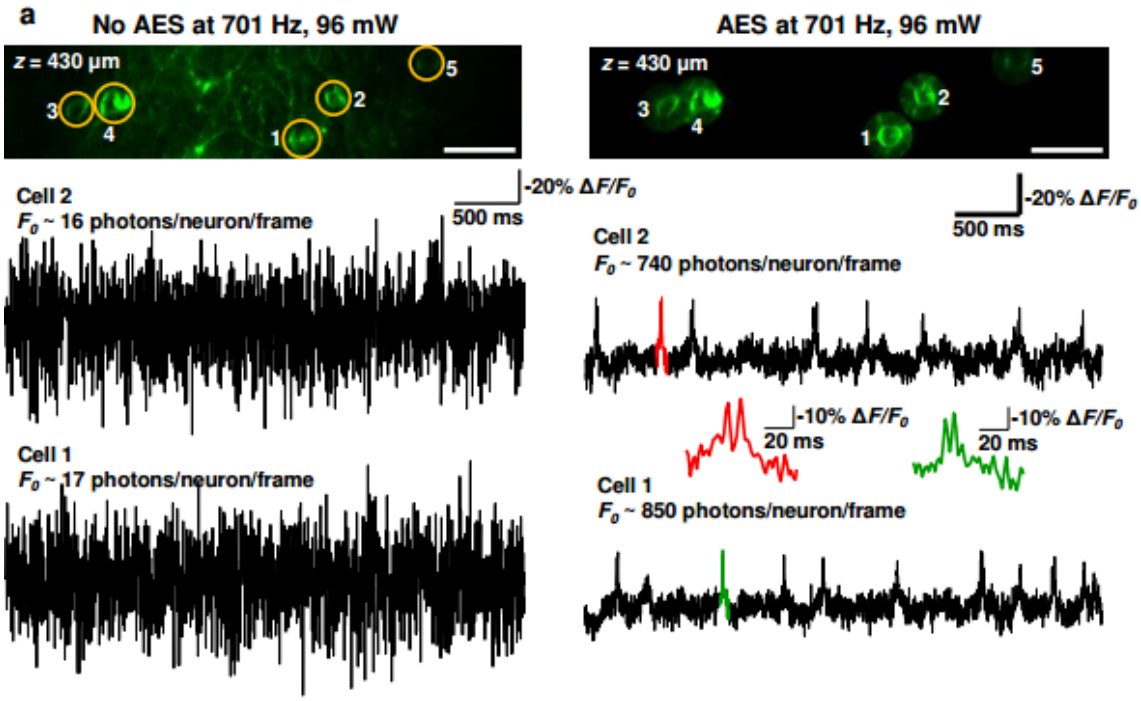

Fig. 3.3 In vivo two-photon imaging of ASAP5 in the mouse visual cortex. The left panel shows the result without the AES system, while the right panel shows the result with AES applied.

Also, we're going to do some photon number estimation here.

doi:10.6342/NTU202501717

Table 3.3 Some experimental parameter in AES article and our in vivo experiment.

	AES	This thesis
Average Power (p_0)	96(mw)	45(mw)
Numerical Aperture (A)	1.05	0.45
Repetition Rate (f_p)	91.4(MHz)	80(MHz)

From Eq. (3.3), the relationship between their emission photon number per pulse n_{e3} and our emission photon number per pulse n_{e0} would be

$$\frac{n_{e3}}{n_{e0}} = \left(\frac{96}{45}\right)^2 \left(\frac{1.05}{0.45}\right)^2 \left(\frac{80}{91.4}\right)^2 = 18.99 \quad (3.6)$$

In Table 3.3, we can see that with their AES system, the average power used in this study was significantly higher compared to the previous two theses, which contributed to improved image brightness.

3.2 In vivo ASAP4e Experiment in SNc

Motivated by these voltage imaging studies, we've also done some in vivo mice experiments with kilohertz-sampling (1300Hz).

3.2.1 Two photon microscopy system

For our kilohertz two-photon microscope, Fig. 3.4 has showed the diagram of our two-photon microscopy system setup. The fast-axis and slow-axis scanner we used are

doi:10.6342/NTU202501717

respectively Resonant scanner (CRS8K) and Galvanometer scanner (Model 6210H).

Due to the setup of our in vivo experiment, a grin rod with 0.5 NA has to be used, so we chose a 10X/NA0.45 objective lens to match the NA of our grin rod.

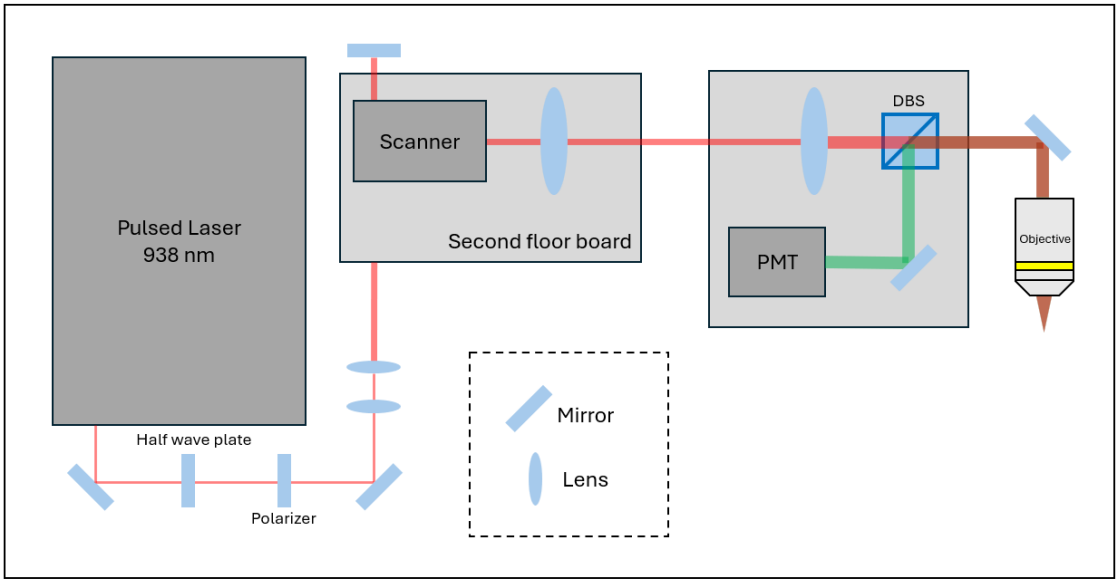

Fig. 3.4 The diagram of our two-photon microscopy system setup.

3.2.2 Mice preparation

Before 3-4 weeks of the experiment started, the ASAP4e virus has already been injected into the mice brain to the SNc region. Meanwhile, the 0.85mm grin rod was also implanted into the same place just being injected. After the surgery, a simple cover made by 3D-printing would be covered on the top of its head, in order to make sure the surface of the grin rod would be well protected during these 3-4 weeks.

14 days later, we could start doing our experiment to the mice at any time.

doi:10.6342/NTU202501717

3.2.3 Experiment Condition

An ASAP4 mice had been prepared for the in vivo experiment. The most important thing of the in vivo experiment, is that the mice must be alive. Although we did the anaesthetization to the mice, we used an IR camera to monitor the breathing of the mice, made sure it was still alive during experiment, as shown in Fig. 3.5

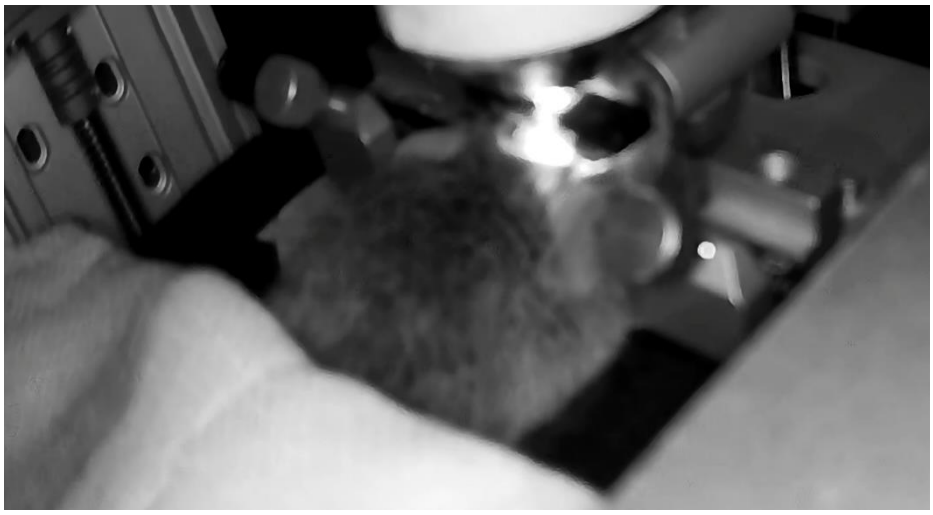

Fig. 3.5 Real time image during in vivo mice experiment. Camera used: FOSCAM C2M

The grin lens was inserted into SNc region of the mice brain. We first adjusted the grin lens position under the objective lens to find the image under grin lens by using low-frame-rate scanning. Fig. 3.6 was the low-frame-rate image under grin lens.

For some experimental condition, the laser repetition rate was 80MHz, the power before the grin rod was set to be 100mW during low frame rate recording, on the other hand 50mW during high frame recording. PMT control voltage was 1.0 (V). The

doi:10.6342/NTU202501717

information of the objective lens and the grin rod we used is shown in Table 3.4 and Table 3.5.

Table 3.4 The parameter of the objective lens we used in the in vivo experiment

Type	MRD70170, Nikon
Immersion	Air
Magnification	10X
Numerical Aperture	0.45
Working Distance (mm)	4

Table 3.5 The parameter of the grin rod we used in the in vivo experiment

Type	NEM-060-50-00-920-s-1.5p
Diameter (mm)	0.85
Length (mm)	7.4
NA	0.5
Pitch	1.5

doi:10.6342/NTU202501717

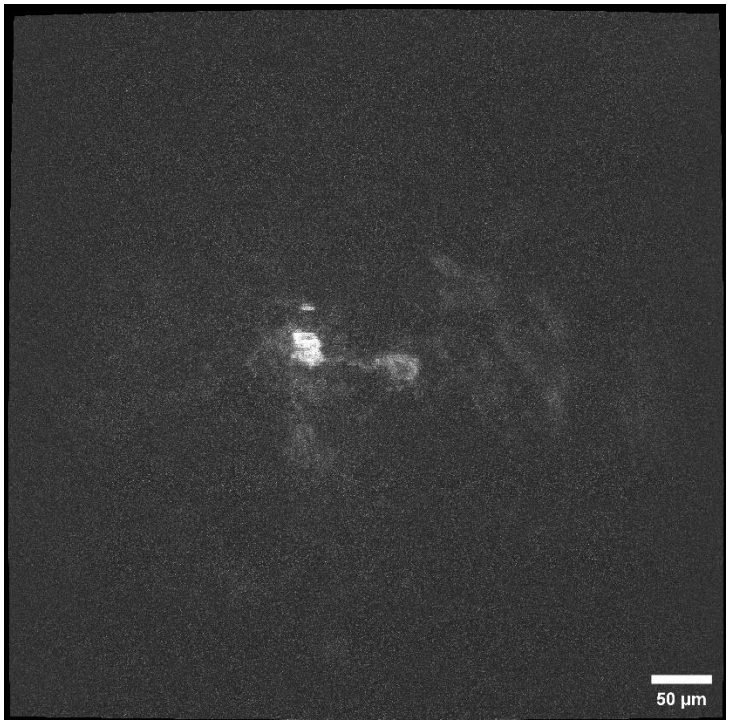

Fig. 3.6 In vivo ASAP4 mice image. Field of view (FOV): 600 x 600µm^2.

After getting the image under grin lens and finding a brain cell with low-frame-rate imaging, we then switched into high-frame-rate scanning and started acquiring image with 1300 Hz frame rate, with about 35 seconds recording time.

3.2.4 Basic Analysis

We have a standard analytical method to our experimental data. Take one of our experimental data for example, we have a sequence of acquired images, which consist of 50000 16-bit gray scale images. Each of their pixel size is 10 x 4793, with about 1300 Hz frame rate, as shown in Fig. 3.7.

doi:10.6342/NTU202501717

Fig. 3.7 Raw image of ASAP4 in vivo mice. The field of view (FOV) was 470 x 20 μm. The pixel number was 10 x 4793. The bitrate was 16-bit (0 – 65535 gray scale).

The first thing we have to deal with the images was to choose the region of interest (ROI). It is very hard for us to select the ROI directly because the raw images are too dark to distinguish the location of the cells, so we have to do some average and contrast processing to the raw images so we can then select the ROI correctly, all these processing were done by ImageJ. Fig. 3.8 is an example of image after these processing

Fig. 3.8 An example of image after we did some average and contrast processing of 50000 frames of raw images.

Then in Fig. 3.8, we can see a donut-shape cell, which is exactly the region of interest (ROI). After selecting the ROI, the pixel size became only 7 x 215 left. There is a very important thing to know before we did the next step, all these processing before, such as average and contrast adjustment, was only by purpose to help us selecting the ROI, the analysis afterward still has to deal with the raw image data.

Next, the most basic analysis of our images, we simply calculate the ΔF/F, which is

doi:10.6342/NTU202501717

a very common analytical method of calcium or voltage imaging.

For the ΔF/F calculation, we first define fluorescence value as the mean value of each frame. F_0, the baseline fluorescence of the trace, was defined as the mean value of the whole fluorescence trace. ΔF was defined as the difference between the fluorescence value of each frame and F_0. And then we get $(F - F_0) / F_0 = \Delta F/F$. In Fig. 3.9, it shows the ΔF/F calculation of Fig. 3.8 's ROI

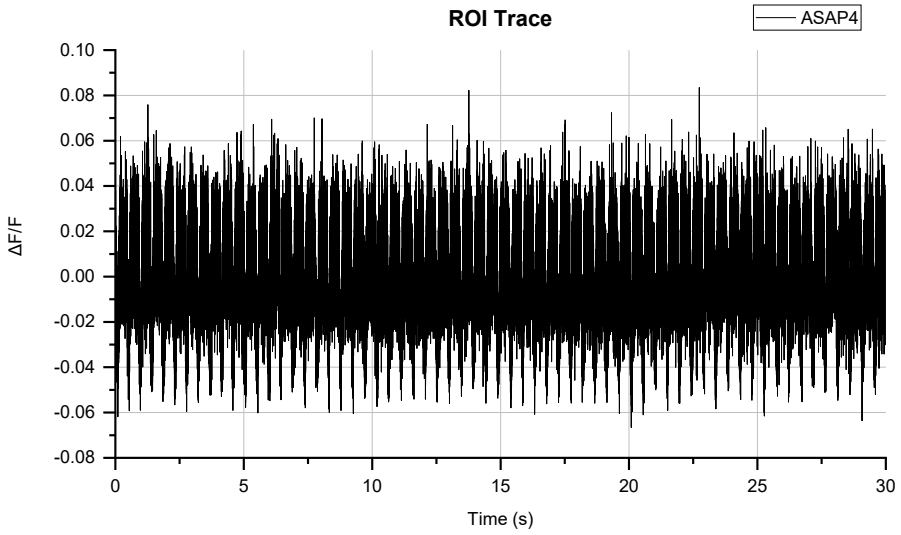

Fig. 3.9 The ΔF/F result of Fig. 3.8 's ROI. The recording time was about 35s.

There is a phenomenon we can notice in Fig. 3.9. Obviously, we can see a periodical fluorescence changing in the figure, whose period was about 0.54s. The reason of that is due to the breathing of the mice, because the mice was alive during experiment.

doi:10.6342/NTU202501717

For the whole trace of ΔF/F temporal data in Fig. 3.9, the maximum fluorescence change was about 8%. In all other experimental data we have, there also exist about 10% or 20% fluorescence change in the recording. Due to the poor signal-to-noise ratio (SNR), it is hard for us to say we saw the action potential (AP) in our experiment.

doi:10.6342/NTU202501717

CHAPTER 4 SIMULATION

4.1 Simulation of measurement system

4.1.1 Perfect measurement system

The goal of the simulation is to isolate the effect of photon statistics on spike detection performance, independent of hardware imperfections. Thus, for the model of our simulation, we basically just set a perfect condition of the measurement system, so we can focus on the issue of the photon statistics. If we are unable to see the action potential signal under perfect measurement system condition, then we can tell it is also impossible to see it in the real-life condition. The total measurement system of the simulation model is shown in Fig. 4.1.

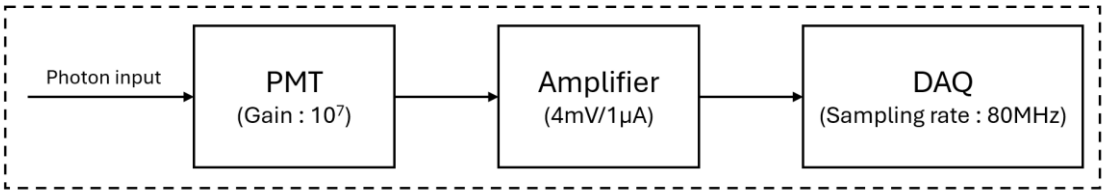

Fig. 4.1 The diagram of the measurement system in our simulation. These setups all depend on our experimental setup.

doi:10.6342/NTU202501717

4.1.2 Photomultiplier tube and amplifier

A perfect-amplification photomultiplier (PMT) was assumed, which amplifies each incident photon with a fixed amplitude. Thus, the photomultiplier (PMT) model was just fairly doing the amplification for every single photon it acquired.

The gain of the photomultiplier tube is set to be 10^7 according to Hamamatsu H11461-03 manual, as shown in Fig. 4.2.

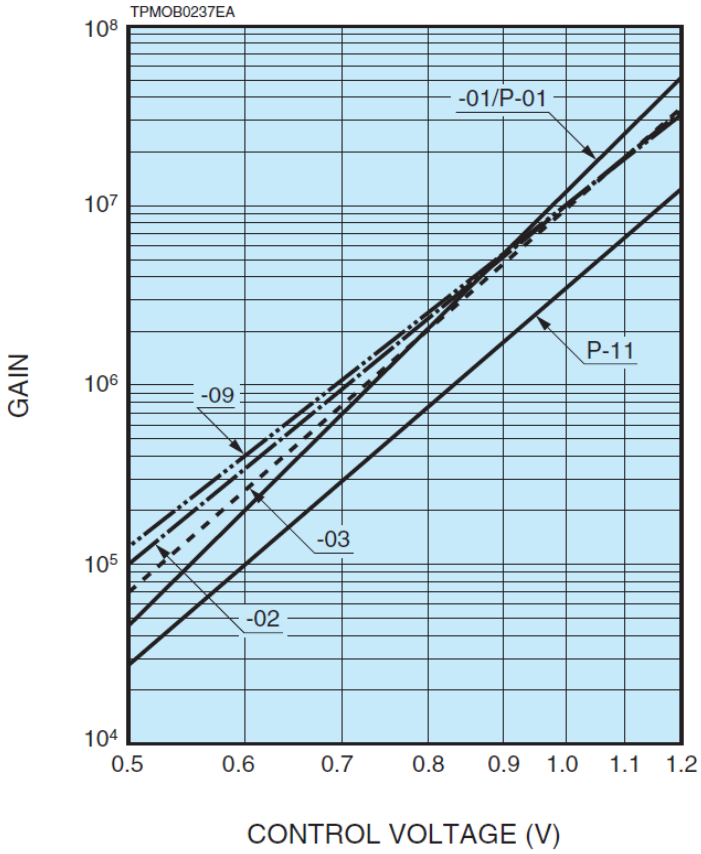

Fig. 4.2 The relationship between photomultiplier tube gain and control voltage. We usually set the control voltage as 1.0 (V) in the experiment, which corresponds to about 10^7 of the gain.

doi:10.6342/NTU202501717

For every single photon input to the photomultiplier tube (PMT), assume that every single photon can be converted into a photoelectron (each charge 1.6 x 10^{-19} coulombs) with 100% quantum efficiency (QE), the output charge of PMT anode would be

$$1.6 \times 10^{-19}(\mathrm{C}) \times 10^{7} = 1.6 \times 10^{-12}(\mathrm{C}) \qquad (4.1)$$

For the anode current output pulse signal, the pulse width was estimated to be 7 ns according to another document from Hamamatsu[4], which talks about some basics and applications of photomultiplier tube (PMT). In a table of this document, it shows that the output pulse width of circular-cage type (Same type as our photomultiplier tube H11461-03) PMT is about 7 ns.

Unit: ns

Dynode type	Rise time	Fall time	Pulse width (FWHM)	Electron transit time	T.T.S.
Linear-focused	0.7 to 3	1 to 10	1.3 to 5	16 to 50	0.37 to 1.1
Circular-cage	3.4	10	7	31	3.6
Box-and-grid	to 7	25	13 to 20	57 to 70	Less than 10
Venetian blind	to 7	25	25	60	Less than 10
Mesh	2.5 to 2.7	4 to 6	5	15	Less than 0.45
Metal channel	0.65 to 1.5	1 to 3	1.5 to 3	4.7 to 8.8	0.4

T.T.S.: Transit Time Spread

Fig. 4.3 Table of some parameters of different type of photomultiplier tube (PMT)

Then the peak current of the output pulse can be estimated as

$$\frac{1.6\times10^{-12}\ (C)}{7\times10^{-9}\ (s)} = 0.229 \times 10^{-3}\ (A) = 228.57\ (\mu A) \qquad (4.2)$$

The current pulse then converted into voltage pulse after an amplifier (Hamamatsu

doi:10.6342/NTU202501717

C9663), which has a conversion factor of 4mV/μA according to the manual, so the output peak voltage becomes

$$228.57\ (\mu A) \times 4\ \left(\frac{mV}{\mu A}\right) = 914.28\ (mV) \qquad (4.3)$$

In conclusion, for every single photon incident into the photomultiplier tube (PMT), it eventually became an electric pulse signal with a 914.28mV amplitude.

4.1.3 Data Acquisition system

For the data acquisition system (DAQ), ATS9440-AlazarTech was used. The sampling rate was adjusted into 80MHz by external clock sampling. The data acquisition system (DAQ) is also assumed to be ideal, sampling the instantaneous voltage values. In other words, for every single photon incident into the photomultiplier tube (PMT), the DAQ would record a 914.28 mV value on a data point. The electrical noise was also ignored in the simulation.

4.2 Random photon generated model

4.2.1 Statistic of photon emission

The simulation now becomes very simple. For the 80MHz pulse laser excitation, and also 80MHz sampling rate, we can simply just consider every single photon emission between 12.5 ns as sequence of random events. We now encounter a serious question: What should the random events statistical model be of the photon emission?

doi:10.6342/NTU202501717

Some studies have shown that the photon emission from single-molecule excitation can exhibit sub-Poisson statistics at nanosecond resolution [5, 8]. However, in the case of our simulation, it is definitely a multi-molecule condition because there must exist much more than one green fluorescent protein (GFP) molecule in a cell. The Sub-Poisson distribution also become simply Poisson distribution during multi-molecule condition [8]. On the other hand, our periodic excitation duration is 12.5 ns, which is about 5 times greater than the fluorescence lifetime of green fluorescent protein (GFP) (about 2.5 ns), so the super-Poisson behavior [9] also wouldn't happen under this condition.

The Poisson distribution is a discrete probability distribution, which is commonly used to describe the distribution of event occurring number in an interval time. Giving the expectation value of a Poisson distribution λ in a certain interval, the probability of k occurring number in the interval is [10]

$$\frac{\lambda^k e^{-\lambda}}{k!} \qquad (4.4)$$

Here, by using Poisson model to generate random photon number for every pulse, we want to emphasize that the photon emission has now been quantized, in low emission photon number condition, the photon quantization plays the significant role for our subsequent simulation result.

doi:10.6342/NTU202501717

4.2.2 Average photon emission rate

In 4.2.1, we've showed that the statistical model of the emission photons can be described as a Poisson distribution model. Then the most important parameter to generate the Poisson random number is the mean value of Poisson distribution λ. In the case of photon emission, it is represented as the average photon emission rate of every laser pulse excitation. We define the photon emission rate per second as λ_{second}. The photon emission rate for every single pulse we define it as u_p.

To set the value of λ in simulation, it was calculated according to the experimental data in Chapter 3 because we want to do the comparison between simulation and experimental result eventually. In 4.1.2 we've showed that for every single input the DAQ would acquire about 914.28 mV average voltage value. Due to this we can estimate back the average photon emission rate by the experimental images.

Take an example of the data in Fig. 3.7, let's only take the part of image sequences that weren't affected by breathing. The image pixels have been changed from voltage value into 16-bit gray scale (0~65535) by 1.0V input range, the gray scale value of a certain pixel assumed to be I_{xy}, x and y represent the pixel location. Then, the corresponding voltage value would be

$$V_{xy}(V) = I_{xy} \times \frac{1.0(V)}{65535}$$

doi:10.6342/NTU202501717

By previous experiment, it has showed that there existed about 4000 gray scale value (~61mV) of the background noise during full-dark condition, so we first did a subtraction for this background value. Then, we did the integration of all the pixels, and for 914.28mV average voltage value for every single acquired photon, the photon number in the ROI would be

$$n_{ROI} = \sum_{y=1}^{y_{max}} \sum_{x=1}^{x_{max}} I_{xy} \times \frac{1000(mV)}{65535} / 914.28(mV) \quad (4.5)$$

And then, the average photon rate for every ROI was simply the mean value of every frames

$$\lambda_{ROI} = mean[n_{ROI}]_{all\ frame} \quad (4.6)$$

And the photon rate per pulse would be

$$\lambda_p = \frac{\lambda_{ROI}}{xy} \quad (4.7)$$

Because there is only part of the pulses irradiate in the ROI, so the photon rate per second would be

$$\lambda_{second} = \lambda_p \times 80e6 \times \frac{ROI\ pixel\ number}{pulse\ number\ per\ frame} \quad (4.8)$$

By this process, the average photon emission rate per pulse u_p was estimated to be 0.0031, during the baseline photon rate we can also call it λ_0. For s_{econd}, in the next section 4.3, we will mention about our experimental frame pulse number and ROI pixel number, then λ_{second} was estimated to be

doi:10.6342/NTU202501717

$$\lambda_{second} = 0.0031 \times 80e6 \times \frac{1505}{61538} = 6065(photon/s) \quad (4.9)$$

An example of simulated trace with $0.0031\lambda_0$ is shown in Fig. 4.4. and Fig. 4.5.

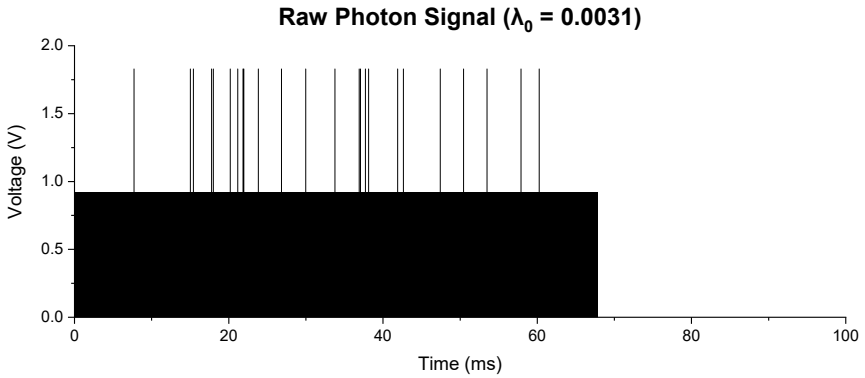

Fig. 4.4 Simulated trace for 100ms photon emission with λ_0 =0.0031, each photon was converted into 914.28mV acquired.

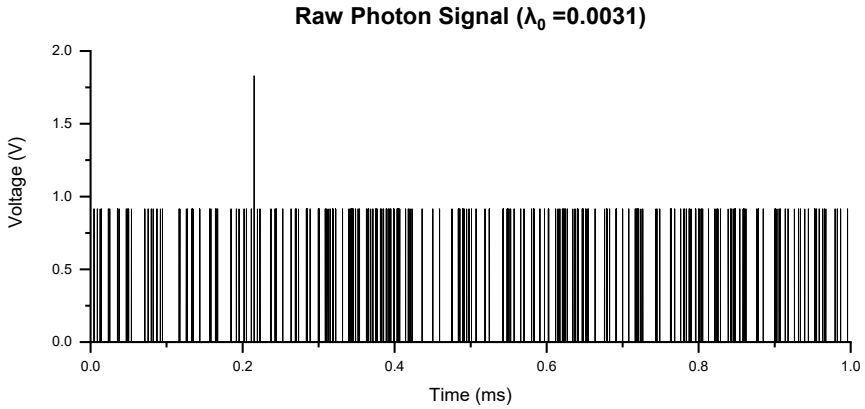

Fig. 4.5 Simulated trace for 1ms photon emission with λ_0 =0.0031.

In Fig. 4.4. and Fig. 4.5, we can obviously see the result brought by quantization of the emission photons.

doi:10.6342/NTU202501717

4.3 Pixel binning

In Fig. 4.4, the trace was obviously seen to be discrete, for $\lambda_0 = 0.0031$, the emission photon number per pulse has a high probability to be 0, sometimes it went to 1 or 2. However, it showed that none of them exceeded 4 photons per pulse in the whole trace of 100ms-simulation.

Thus, just like we did to the experimental images, pixels should be binned together for the next step. In the case of our experimental parameter, due to the fix distortion method of the raw images, originally the theoretical pixel number along x axis should be

$$x\ axis\ pixel\ number = \frac{Laser\ repetition\ rate}{resonant\ scanner\ frquansy \times 2} = \frac{80(MHz)}{8k \times 2} = 5000 \qquad (4.10)$$

However, by the fix distortion method to our images, several pixels from the two sides of the images were abandoned, the x axis pixel number remained only 4793.

For the recording frame rate, the theoretical frame rate should be

$$frame\ rate = \frac{1}{\frac{1}{resonant\ scanner\ frequansy \times 2} \times y\ axis\ pixel\ number}$$

$$= \frac{1}{\frac{1}{8k \times 2} \times 10} = 1600(Hz) \qquad (4.11)$$

However, there are still some reasons such as electronic delay and unideal scanner movement, made it lower in the real condition. In reality, the frame rate eventually became about 1300Hz, which mean it actually wasted a little time during sampling.

doi:10.6342/NTU202501717

In the simulation, let's assume a 1300 fame rate experimental condition, there cost accordingly 80e6/1300 = 61538 pulses for every frame. However, if we ignore the abandoned pixels by fix distortion method, there exist 10*5000 = 50000 pixels for every single frame, which mean there are 1538 pulses wasted. Then for each 50000 pixels in a single image, only 1505 of them were in the region of interest (ROI) (experimental pixel number in ROI), thus we did the binning of 1505 data points for every 61538data points, and the frame rate would be 1300Hz. The result after binning would be shown in Fig. 4.6.

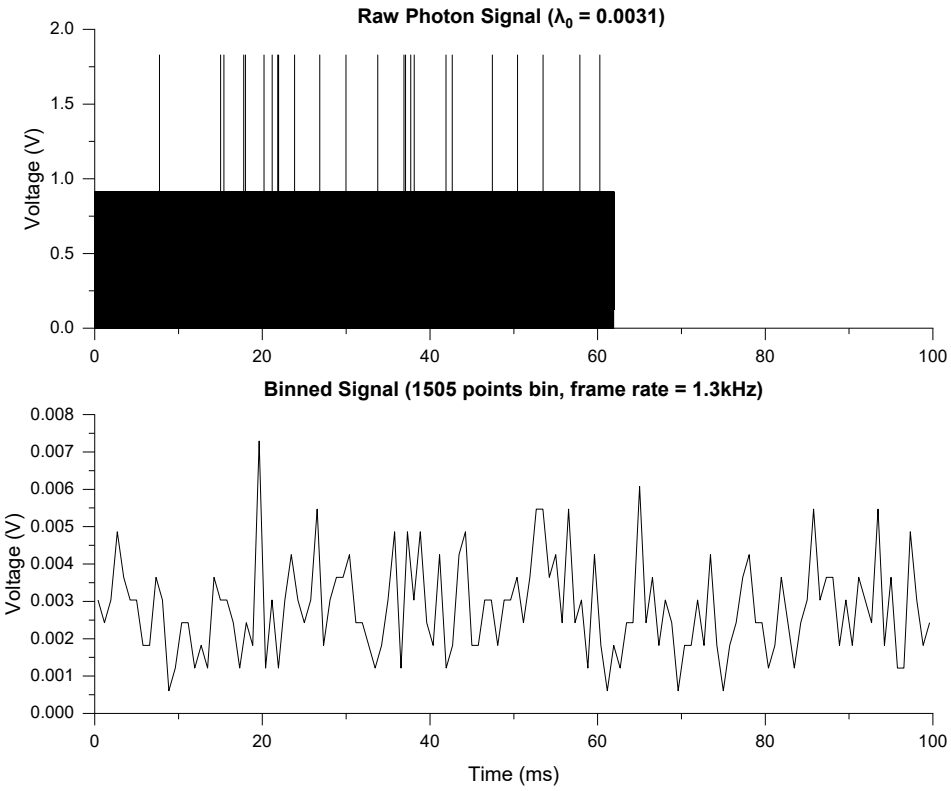

Fig. 4.6 The binning result of Fig. 4.4, for each 61538 data points, 1505of them was

doi:10.6342/NTU202501717

binned.

The bin number N is an important variable in our simulation. In the experiment, it indicates the ROI pixel number, which can affect the signal-to-noise ratio (SNR) and the spike detected rate directly.

4.4 Spike signal added

After the basic photon emission simulation has been successfully established, some action potential spikes can be added in the simulation. For a 30-second simulation, we totally add 100 spikes into it to see if these spikes can be detected. For every added spike, a gaussian-curve with 1ms FWHM was used. The amplitude of the spikes according to some research about voltage imaging would be about 120% of the baseline brightness.

Based on the definition of ΔF/F, ΔF during spike peak represents the difference between peak amplitude and the baseline rest value. F, also called F_0, represents the baseline brightness during resting. Thus ΔF/F of the spike is

$$\frac{\Delta F_{AP}}{F_0} = \frac{F_{AP} - F_0}{F_0} \qquad (4.12)$$

In our simulation, Analogous to the definition of ΔF/F, we define the photon rate change as $\Delta\lambda_{AP}/\lambda_0$.

doi:10.6342/NTU202501717

$$\frac{\Delta\lambda_{AP}}{\lambda_0} = \frac{\lambda_{AP}-\lambda_0}{\lambda_0} \quad (4.13)$$

In the results of [14] about ASAP4e volage imaging, the value of $\Delta F_{AP}/F_0$ can be about 10~40%, so the $\Delta\lambda_{AP}/\lambda_0$ of the spikes greater than 10% was also used in our simulation. For example, if the photon rate during baseline λ_0 being 0.0031(photon/pulse) as we estimated in 4.2.2, for 20% photon rate difference in the peak, The peak photon rate λ_{AP} would be

$$\lambda_{AP} = \lambda_0 \times (1 + 20\%) = 0.0031 \times 1.2 = 0.00372(\text{photon/pulse}) \quad (4.14)$$

The curve of the added 20% spike can be showed as in Fig. 4.7

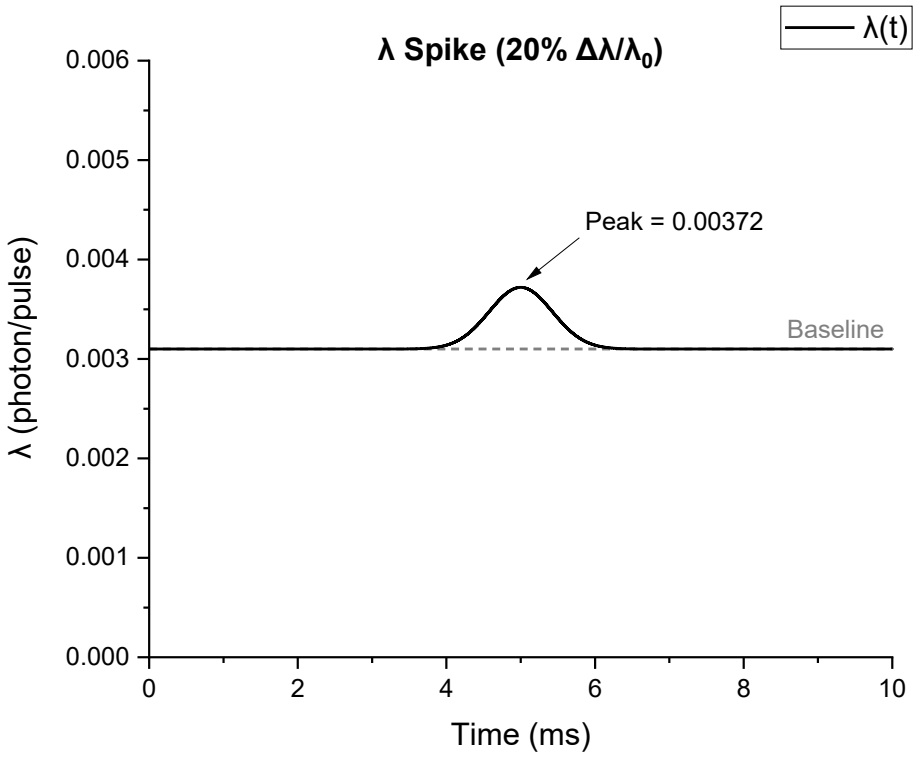

doi:10.6342/NTU202501717

Fig. 4.7 An added spike with 1ms FWHM with 20% $\Delta\lambda_{AP}/\lambda_0$

Using these parameters, we simulated the 30-second photon emission trace, and show the simulation result before and after the spikes were added, as shown in Fig. 4.8.

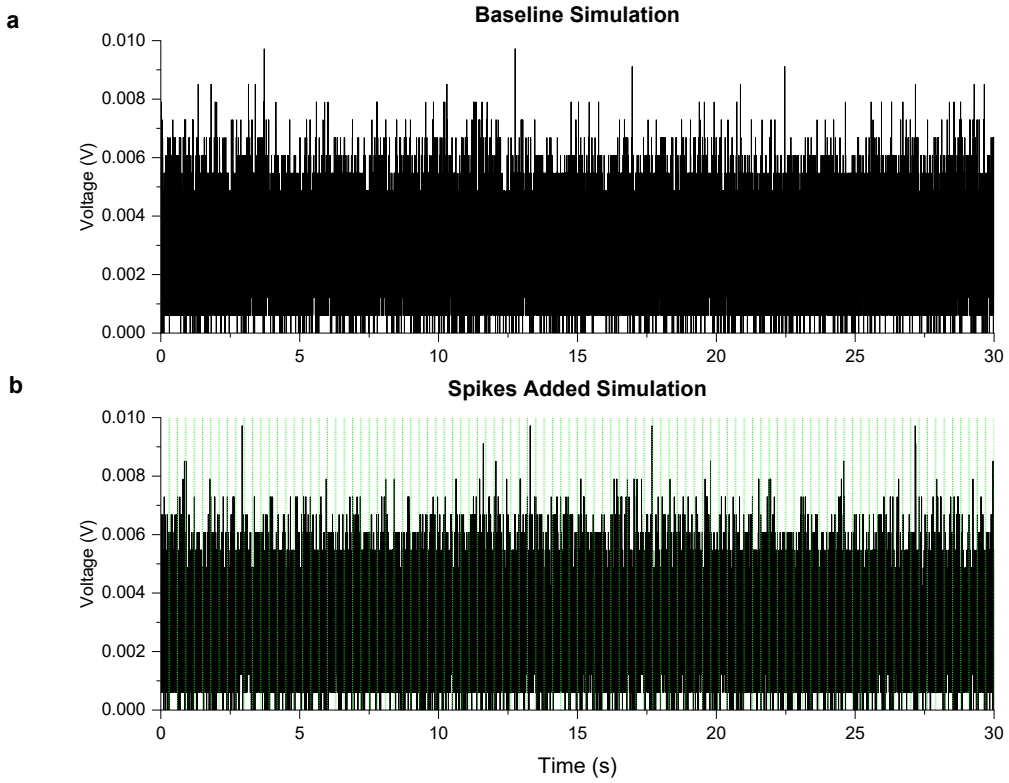

Fig. 4.8 Simulated photon emission trace for 30 seconds. (a) 30-second simulation trace with the pure baseline for $\lambda_0 = 0.0031$. (b) 30-second simulation trace with 100 spikes added at a frequency of one spike every 300ms, the green dashed lines indicate the locations of the added spikes. Simulation parameter: $\lambda_0 = 0.0031$, N = 1505, $\Delta\lambda_{AP}/\lambda_0$ = 20%.

doi:10.6342/NTU202501717

The result in Fig. 4.8 showed that under these parameter settings, the difference was indiscernible after the spikes added.

doi:10.6342/NTU202501717

CHAPTER 5 RESULT

5.1 Spike detected

5.1.1 The method of spikes detection

After acquiring the result of 30s simulation in Fig. 4.8, an important thing to do in the next step was to see if these added spikes could be detected. Thus, based on a study about voltage imaging[17], which adopted a rigorous approach to detect the spike for their fluorescence trace result. The spike events have to jointly satisfy three equations:

$$dF_{ur}(t) > mean[dF_{ur}(t_0)]_{|t_0-t|<1s} + 3 \times std[dF_{dr}(t_0)]_{|t_0-t|<1s} \quad (5.1)$$

$$F_{detrend}(t) > mean[F_{detrend}(t)]_{t_0-t<0.1s} + 3 \times \sigma_F(t) \quad (5.2)$$

$$F_{AP}(t) > 4 \times \sigma_F(t) \quad (5.3)$$

The details of these three equations have been thoroughly described in [17].

5.1.2 True positive (TP), false positive (FP) and false negative (FN)

Let's analyze a 30s-simulation with these equations. Take the same simulation parameters we did in Fig. 4.8, the result should be shown in Fig. 5.1.

doi:10.6342/NTU202501717

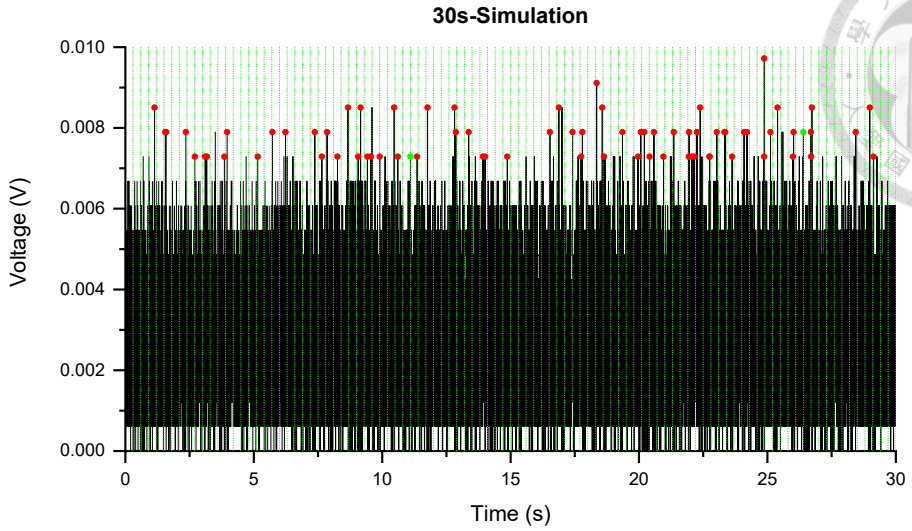

Fig. 5.1 Simulation result with spike detected method. The green dots represent those added spikes that have been successfully detected. Red dots represent the locations in the baseline who were mistakenly detected.

In the result of Fig. 5.1, the green dots represent true positives (TP), which are the spikes that were successfully detected at the correct position where artificial spike signals were added, while the red dots indicate false positives (FP), where signals were mistakenly detected in the baseline (non-spike) regions. Also, for those spikes that were artificially added but not successfully detected, we can call them false negatives (FN).

5.2 Sensitivity and precision

Due to the stochastic property of simulated photon emission, a single 30-second simulated trace wouldn't be enough for analysis, each simulation result can be different.

doi:10.6342/NTU202501717

Therefore, for each set of the simulation, we performed 10 independent 30-second simulations.

To fairly evaluate these simulation results, we would like to adopt two important metrics: sensitivity and precision.

Sensitivity represents the proportion of the successfully detected spike among all the artificially added spikes. By adopting some indicators in 5.1.2, the value of sensitivity can be represented as

$$Sensitivity = \frac{TP}{TP+FN} \quad (5.4)$$

On the other hand, precision indicates that among all of these detected spikes, in what proportion of them are the real spikes.

$$Precision = \frac{TP}{TP+FP} \quad (5.5)$$

Both sensitivity and precision are important metrics for evaluating spike detection performance. Poor sensitivity indicates a poor detection rate of true spike signals, while low precision implies a high number of false positives, which may obscure or mislead the interpretation of the actual signal.

5.3 Result

5.3.1 Variables of simulation

In the simulation, there are three tunable parameters: the photon rate (λ_0), Bin

doi:10.6342/NTU202501717

number (N) and the photon rate change of the spikes ($\Delta\lambda_{AP}/\lambda_0$), which have been introduced in 4.2.2, 4.3 and 4.4 respectively. We first set $\lambda_0 = 0.0031$ (photon/pulse) and $N = 1505$ based on experimental data, and $\Delta\lambda_{AP}/\lambda_0$ was set to be 20%, which was about the value from some GEVI related studies. Then, to see the influence of each variable individually, we performed our simulations by varying one of the variables at a time. For each setting, we performed 30-second simulation for ten times and summarized the average and standard deviation of both sensitivity and precision. Table 5.1 shows the results of a 30-second simulation.

doi:10.6342/NTU202501717

Table 5.1 The results of 30-second simulation for ten times with λ_0 =0.0031, N = 1505 setting from experimental data and $\Delta\lambda_{AP}/\lambda_0$ = 20%.

						Average		Std	
	TP	FP	FN	Sensitivity	Precision	Sensitivity	Precision	Sensitivity	Precision
Ⅰ	2	80	98	2.00%	2.44%	2.00%	2.69%	1.33%	1.81%
Ⅱ	1	84	99	1.00%	1.18%				
Ⅲ	2	59	98	2.00%	3.28%				
Ⅳ	1	70	99	1.00%	1.41%				
Ⅴ	1	69	99	1.00%	1.43%				
Ⅵ	1	70	99	1.00%	1.41%				
Ⅶ	3	79	97	3.00%	3.66%				
Ⅷ	5	68	95	5.00%	6.85%				
Ⅸ	1	76	99	1.00%	1.30%				
Ⅹ	3	72	97	3.00%	4.00%				

5.3.2 Results with variation of photon rate (λ_0)

Here we first investigate how photon emission rate influences the sensitivity and precision of spikes detection. Based on the experimental data, in 4.2.2 showed that the photon rate per pulse (λ_0) = 0.0031 (photon/pulse). We varied the photon rate (λ_0) across a range from 0.000625 to 0.25, with experimental setting λ_0 = 0.0031 included. The diagrams from Fig. 5.2 and Fig. 5.3 shows the results of spike detection sensitivity and precision.

doi:10.6342/NTU202501717

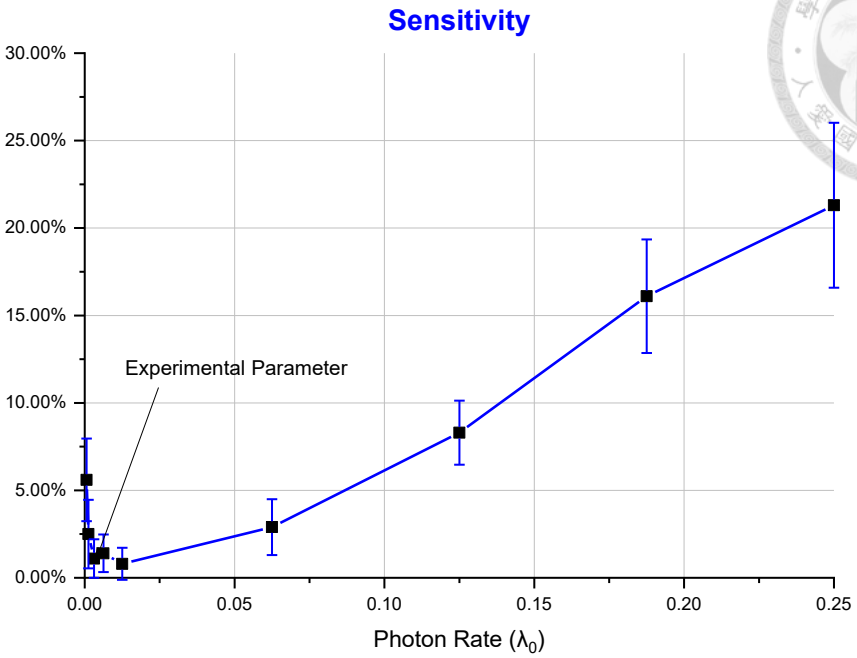

Fig. 5.2 The diagram shows relationship between sensitivity and photon rate (λ_0). The sensitivity values (mean ± standard deviation) were obtained from ten independent simulations at each photon rate. The position of the experimental photon rate has also been marked. The simulation code is provided in appendix A.

doi:10.6342/NTU202501717

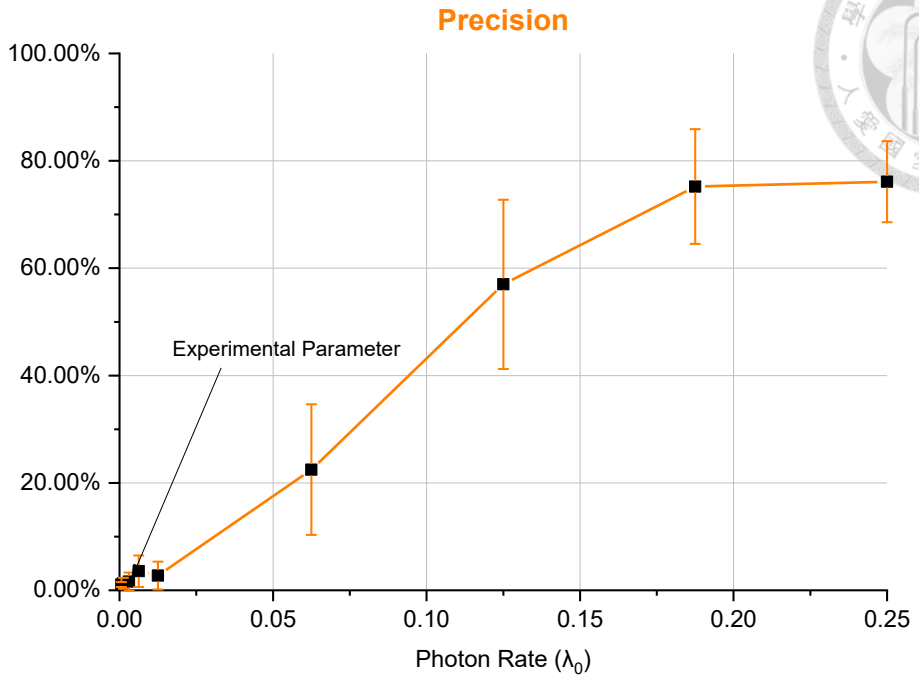

Fig. 5.3 The diagram shows relationship between precision and photon rate (λ_0). The precision values (mean ± standard deviation) were obtained from ten independent simulations at each photon rate. The simulation code is provided in appendix A.

As shown in Fig. 5.2, the sensitivity generally shows a positive correlation with the photon rate (λ_0). However, a slight inverse trend can be observed at low photon rates. This phenomenon can be further explained in the later section some theoretical derivations of sensitivity. In contrast, as shown in Fig. 5.3, the precision shows a consistently positive correlation with photon rate across the entire diagram.

In summary, increasing the photon rate clearly enhances both sensitivity and

doi:10.6342/NTU202501717

precision, indicating that image brightness plays a crucial role in improving spike detection performance.

5.3.3 Results with variation of bin number (N)

This section then explores the impact of bin number (N) (i.e., the pixel number of the region of interest (ROI)) on the detection sensitivity and precision. The experimental bin number is N = 1505. Including this, we varied bin number (N) across the range from 200 to 38400, N = 38400 was the maximum bin number setting, which indicates that all the pixels are totally being used. The diagrams from Fig. 5.4 and Fig. 5.5 shows the result of spike detection sensitivity and precision.

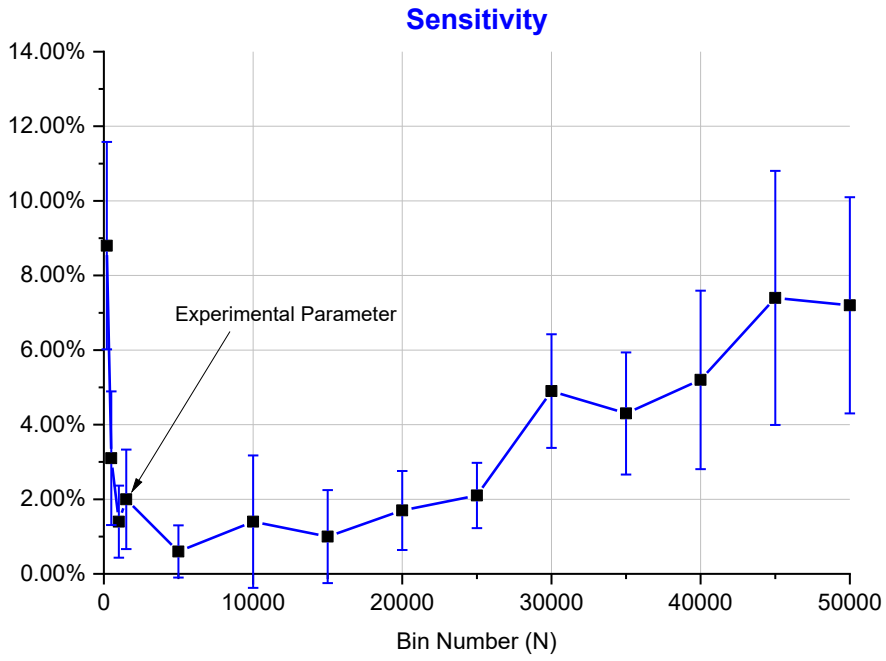

Fig. 5.4 The diagram shows relationship between sensitivity and bin number (N). The

doi:10.6342/NTU202501717

sensitivity values (mean ± standard deviation) were obtained from ten independent simulations at each bin number. The position of the experimental photon rate has also been marked. The simulation code is provided in appendix B.

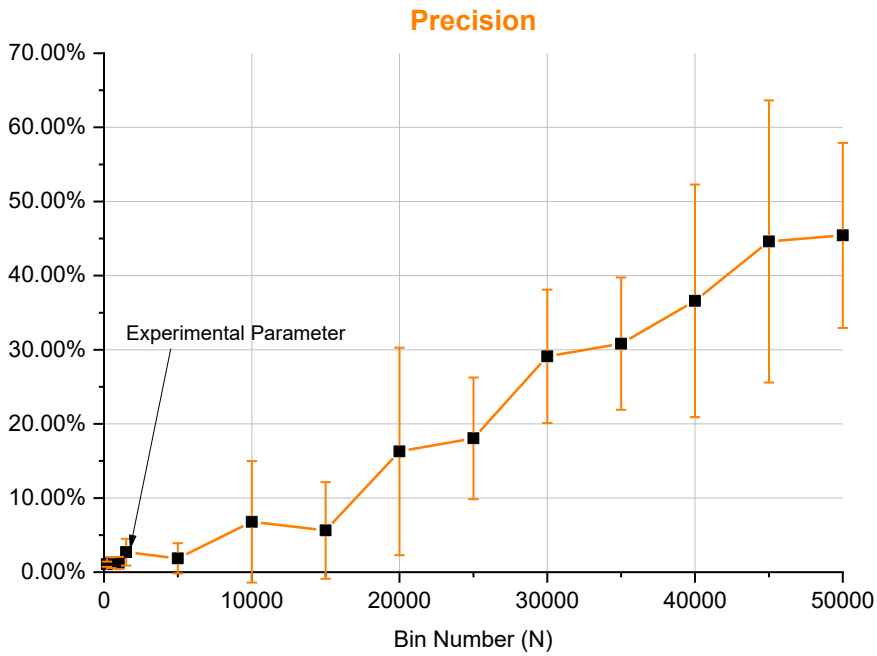

Fig. 5.5 The diagram shows relationship between precision and bin number (N). The precision values (mean ± standard deviation) were obtained from ten independent simulations at each bin number. The simulation code is provided in appendix B.

The trends shown in both the sensitivity and precision plot in Fig. 5.4 and Fig. 5.5 are very similar to those observed in 5.3.2. In particular for the diagram of sensitivity, an inverse trend can be observed in both low photon rate and low bin number.

doi:10.6342/NTU202501717

5.3.4 Results with variation of spike photon rate change ($\Delta\lambda_{AP}/\lambda_0$)

In this section we are going to investigate impact from the last variable, spike photon rate change ($\Delta\lambda_{AP}/\lambda_0$). Studies about voltage imaging show that the fluorescence change ($\Delta F/F_0$) in the range of about 10%~40%. We varied the spike photon rate change ($\Delta\lambda_{AP}/\lambda_0$) across a range from 10% to 120%. The diagrams from Fig. 5.6Fig. 5.2 and Fig. 5.7 shows the result of spike detection sensitivity and precision.

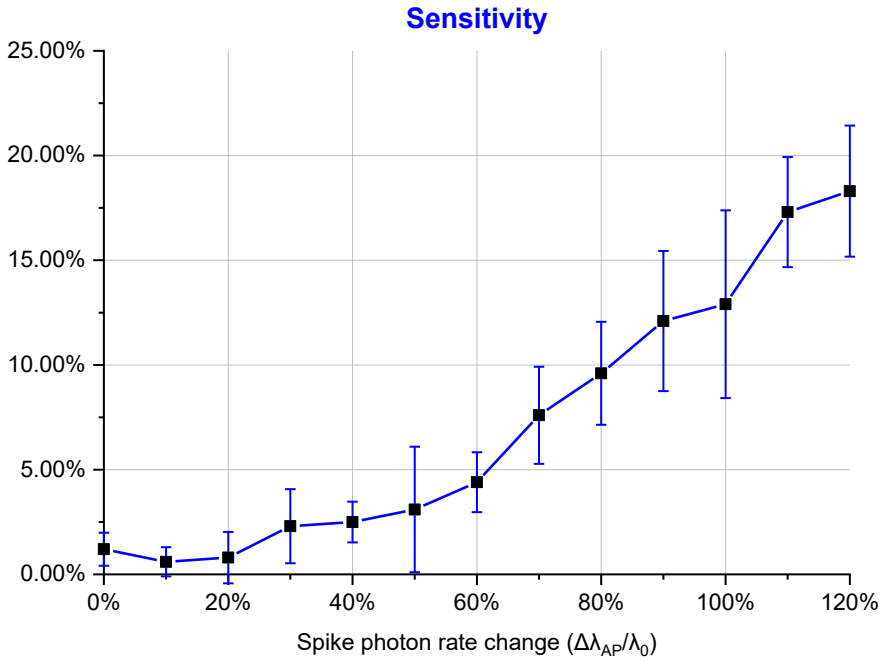

Fig. 5.6 The diagram shows relationship between sensitivity and spike photon rate change ($\Delta\lambda_{AP}/\lambda_0$). The sensitivity values (mean ± standard deviation) were obtained from ten independent simulations at each spike photon rate change ($\Delta\lambda_{AP}/\lambda_0$). The simulation code is provided in appendix C.

doi:10.6342/NTU202501717

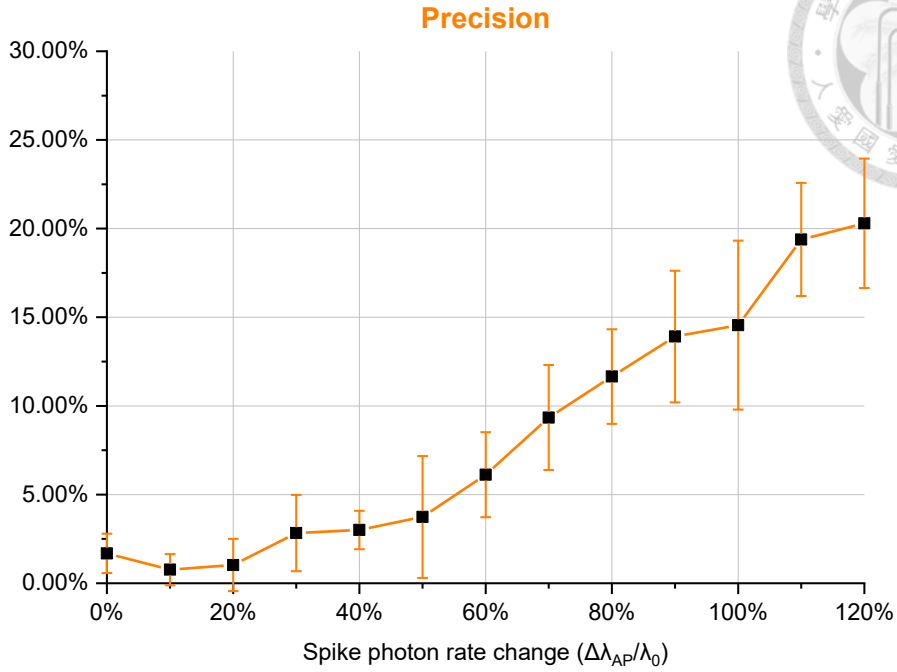

Fig. 5.7 The diagram shows relationship between precision and spike photon rate change ($\Delta\lambda_{AP}/\lambda_0$). The precision values (mean ± standard deviation) were obtained from ten independent simulations at each spike photon rate change ($\Delta\lambda_{AP}/\lambda_0$). The simulation code is provided in appendix C.

Unlike the result in 5.3.2 and 5.3.3, the sensitivity diagram in Fig. 5.6 doesn't show inverse trend at low section, but a consistently positive correlation in the whole section, same as the diagram of precision result.

5.4 Theoretical sensitivity and precision

The results of sensitivity in 5.3.2 and 5.3.3 have shown some inverse trend during

doi:10.6342/NTU202501717

either in low photon rate (λ_0) or low bin number (N). Let's try to explain this phenomenon in a theoretical way. The precise value of the sensitivity was hard to estimate by three spike detection formulas in 5.3.1. However, we can estimate the trend of the relationship between sensitivity and photon rate (λ_0) or bin number (N).

5.4.1 Theoretical sensitivity

The main reason why the spike detection sensitivity inversely became higher during low photon rate (λ_0) was because of the spike detection formula mentioned in 5.1.1. When the photon rate becomes lower, the threshold value also becomes lower due to its connection to the stander deviation of the trace. Here we're going to estimate the theoretical sensitivity, it is hard to estimate the precise value but we can show if the trend be similar with the simulation result.

In Eq. (5.2), we can consider the equation simply as a constant threshold condition

$$F(t)_{AP} > mean[F(t)_{baseline}] + 3 \times std[F(t)_{baseline}] \quad (5.6)$$

The time window of 0.1ms during calculating the mean value was smaller than the periodic duration we gave to the added spike (0.3ms), so the time window can be ignored here.

Then, we first calculate the threshold. In the simulation, with the bin number N and photon rate λ_0, by the definition of Poisson distribution, the mean value and the standard

doi:10.6342/NTU202501717

deviation of the raw baseline trace would be

$$mean[F(t)_{raw}] = \lambda_0 \quad (5.7)$$

$$std[F(t)_{raw}] = \sqrt{\lambda_0} \quad (5.8)$$

By N data points binning, the mean value remained the same, but the standard deviation becomes

$$std[F(t)_{bin}] = \frac{\sqrt{\lambda_0}}{\sqrt{N}} = \sqrt{\frac{\lambda_0}{N}} \quad (5.9)$$

Thus, the threshold value would be

$$Threshold = \lambda_0 + 3\sqrt{\frac{\lambda_0}{N}} \quad (5.10)$$

For the possibility of the added spikes, it can be described as a Poisson possibility mass function with photon rate λ_{AP}

$$P(X = k) = \frac{{\lambda_{AP}}^k e^{-\lambda_{AP}}}{k!} \quad (5.11)$$

After N data points binning, it becomes

$$P(X = k) = \frac{(N\lambda_{AP})^k e^{-N\lambda_{AP}}}{N(k!)} \quad (5.12)$$

By normalize these functions by N, the sensitivity can now consider as the region of a possibility mass function

$$P(X = k) = \frac{(N\lambda_{AP})^k e^{-N\lambda_{AP}}}{k!} = Poisson(\mu = N\lambda_{AP}) \quad (5.13)$$

beyond the threshold value, which should be rounded to the nearest integer

$$Threshold = ceil[N(\lambda_0 + 3\sqrt{\frac{\lambda_0}{N}})] = ceil[N\lambda_0 + 3\sqrt{N\lambda_0}] \quad (5.14)$$

doi:10.6342/NTU202501717

Combined with the concept of the cumulative distribution function, the theoretical sensitivity would be

$$sensitivity = 1 - PoissonCDF(Threshold - 1; \mu = N\lambda_{AP}) \quad (5.15)$$

Where μ is the expected number of the Poisoned.

In Fig. 5.8 and Fig. 5.9, we plot the diagrams of the relationship between the theoretical sensitivity and respectively N and λ.

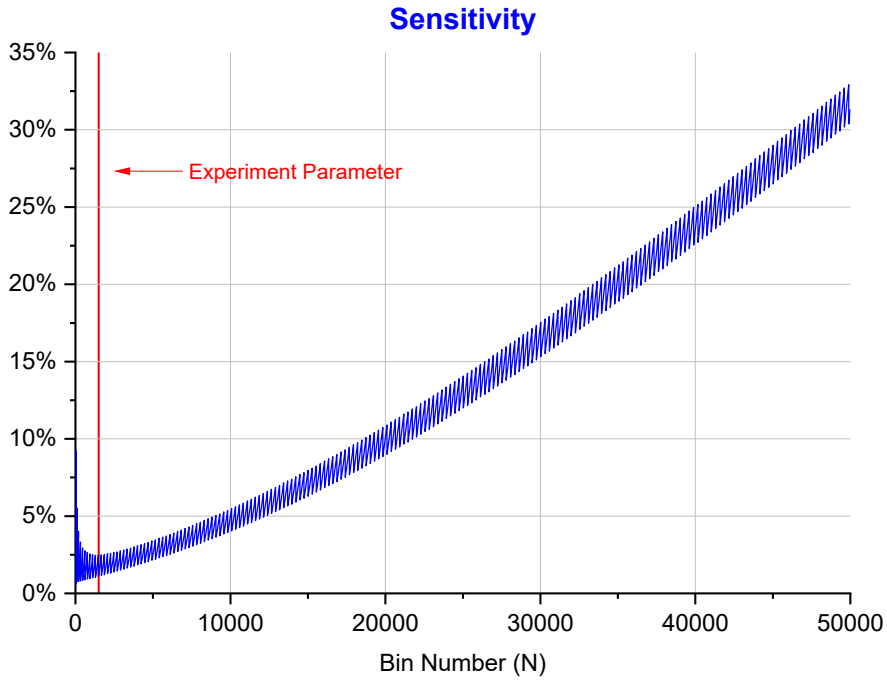

Fig. 5.8 The correlation diagram between theoretical sensitivity and bin number (N).

doi:10.6342/NTU202501717

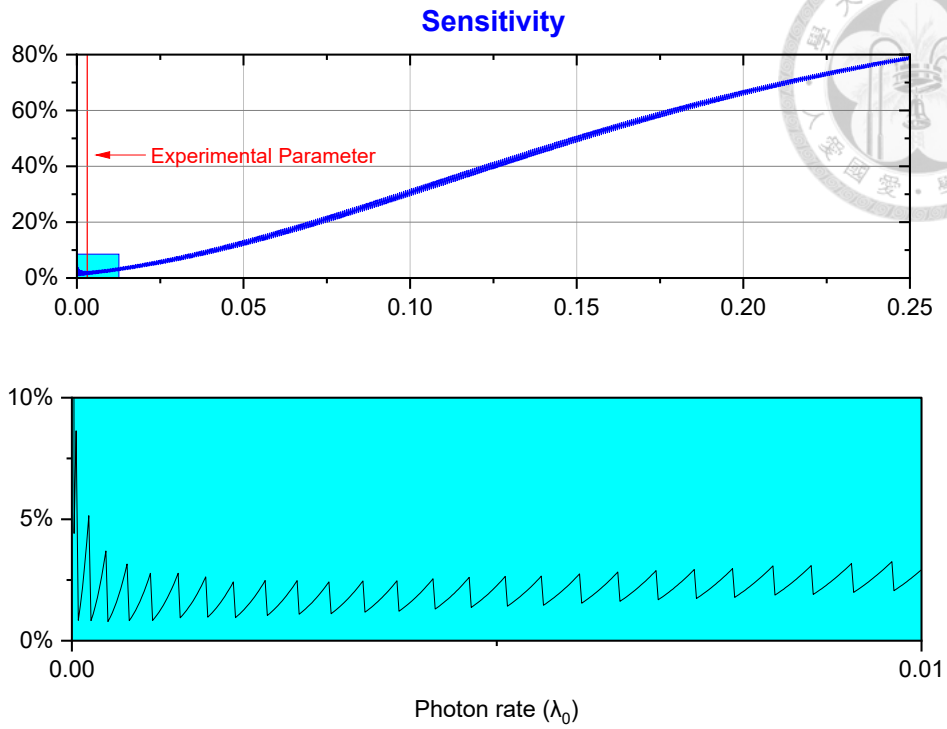

Fig. 5.9 The correlation diagram between theoretical sensitivity and photon rate (λ_0).

It shows that in both Fig. 5.8 and Fig. 5.9, the inversed trend did be observed during low N or low λ, which actually matches the phenomenon observed in the result of Fig. 5.2 and Fig. 5.4. Also, a zigzag-trend was showed in the both diagrams, so the sensitivity wouldn't be consistently growing up.

5.4.2 Theoretical precision

Similar with the estimation of sensitivity, the precision just additionally considers the false positive rate (FPR) of the fake spikes. In the simulation, with totally N_{total} data points (After binning), and N_{AP} added spikes, the theoretical precision would be

doi:10.6342/NTU202501717

$$precision = \frac{TP}{TP+FP} = \frac{sensitivity \times N_{AP}}{sensitivity \times N_{AP} + FPR \times (N_{total} - N_{AP})} \quad (5.16)$$

And the false positive rate (FPR), similar with Eq. (5.15)

$$FPR = 1 - PoissonCDF(Threshold - 1; \mu = N\lambda_0) \quad (5.17)$$

Fig. 5.10 and Fig. 5.11showed the diagram of the theoretical precision.

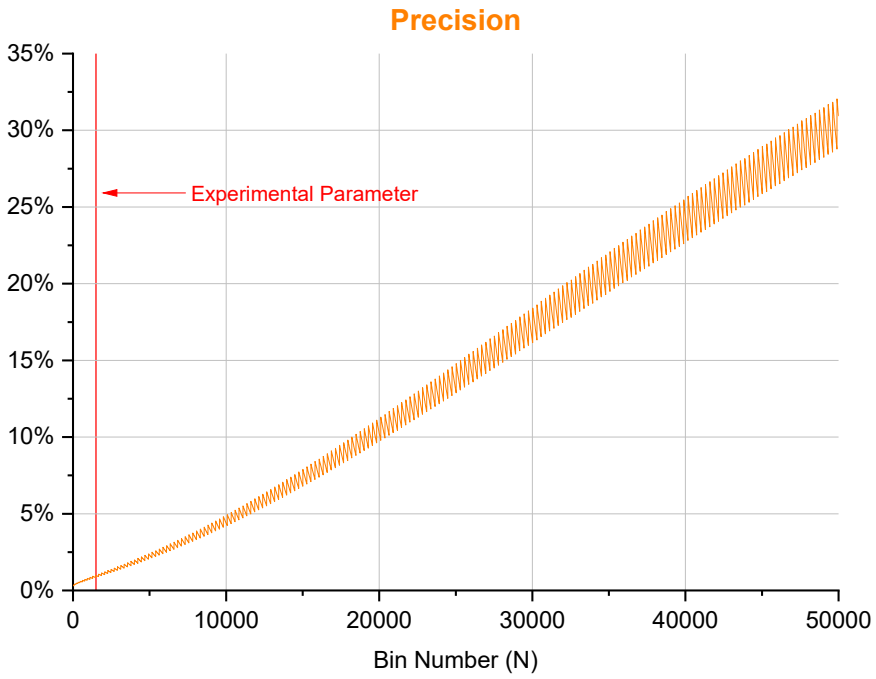

Fig. 5.10 The correlation diagram between theoretical precision and bin number (N).

doi:10.6342/NTU202501717

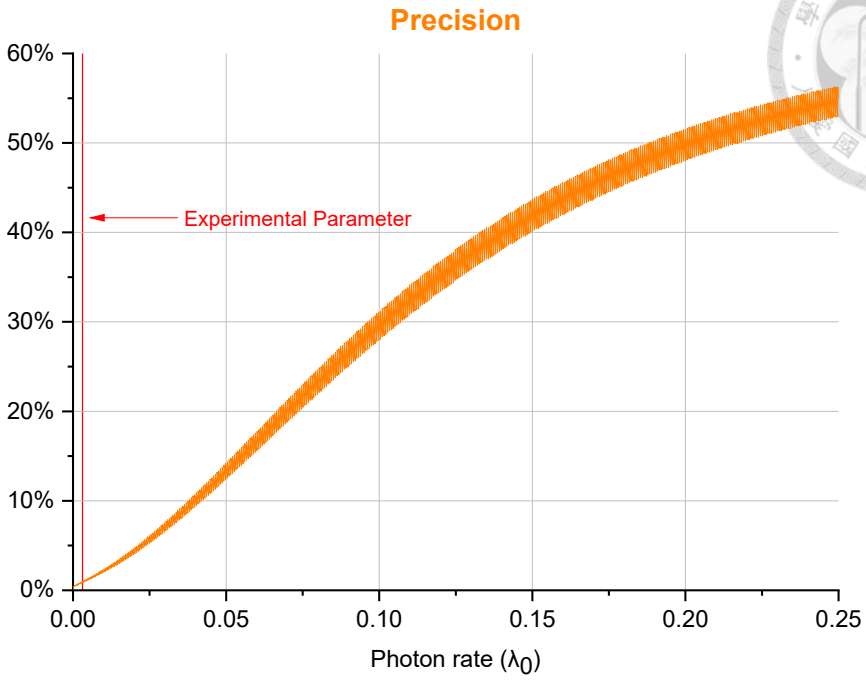

Fig. 5.11 The correlation diagram between theoretical precision and photon rate (λ_0).

The zigzag-trend can also be observed here, but it didn't show the inversed trend during low N value.

5.5 Extended result

In the section of 5.4, if we consider the value of λ_{AP} as λ_0 times a constant A, then

$$sensitivity = 1 - PoissonCDF(ceil[N\lambda_0 + 3\sqrt{N\lambda_0}] - 1; \mu = AN\lambda_0) \quad (5.18)$$

We can now see an interesting thing, the sensitivity and precision are directly being affected by the value of $N\lambda_0$, which also represents the ROI photon rate in each single frame. Combining the result of Fig. 5.2 and Fig. 5.4, we jointly plot them with the value

doi:10.6342/NTU202501717

of $N\lambda_0$ in Fig. 5.12.

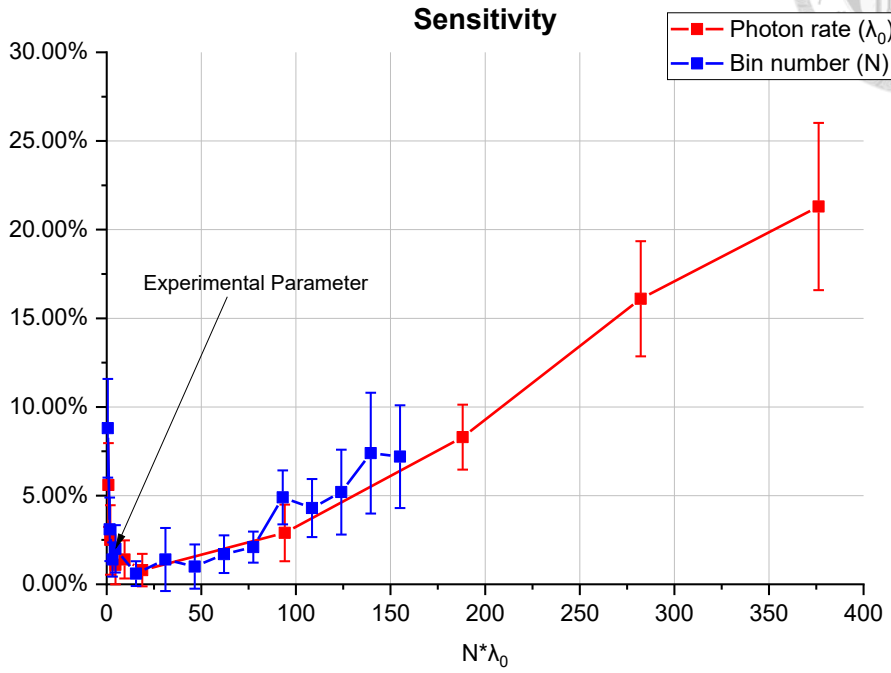

Fig. 5.12 The theoretical sensitivity diagram by combine the results from Fig. 5.2 and Fig. 5.4. Their x-axis value has both been converted into $N*\lambda_0$.

The combination diagram of precision is also shown in Fig. 5.13.

doi:10.6342/NTU202501717

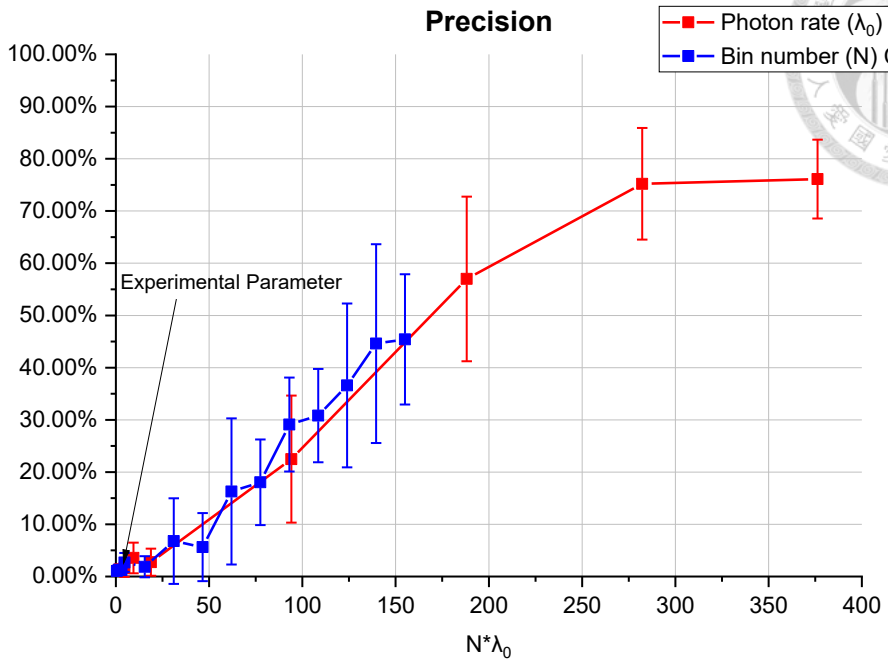

Fig. 5.13 The theoretical precision diagram by combine the results from Fig. 5.3 and Fig. 5.5. Their x-axis value has both been converted into $N*\lambda_0$.

Next, combine these two parameters into only one, there remain only two variables now, which are $N\lambda_0$ and $\Delta\lambda_{AP}/\lambda_0$. We can now show a visualized diagram of the correlation between the simulated sensitivity and these two parameters, as shown in Fig. 5.14

doi:10.6342/NTU202501717

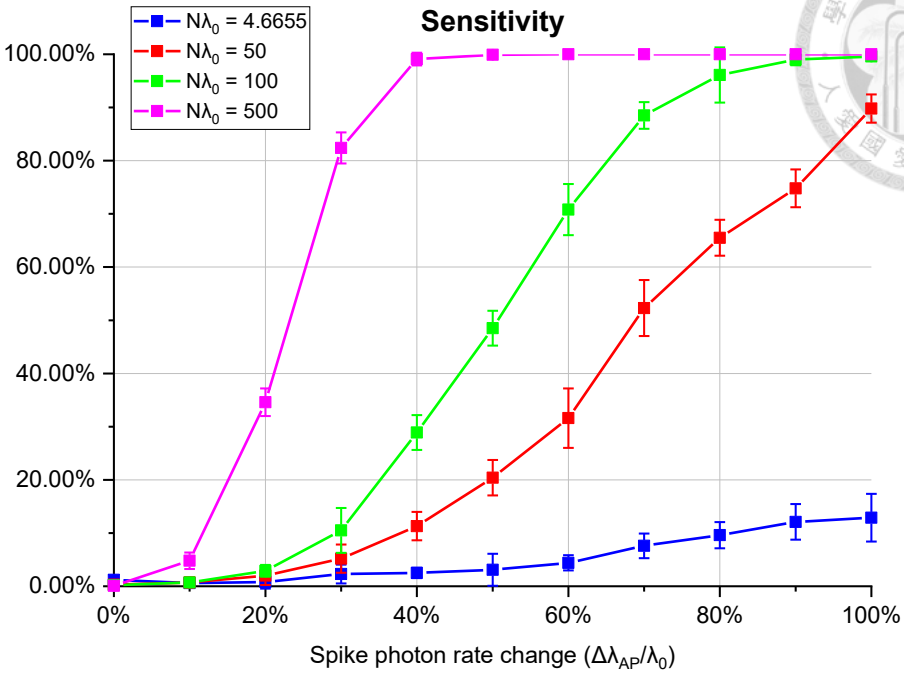

Fig. 5.14 The sensitivity diagram of the simulation result under different $N\lambda_0$. The blue curve indicates the experimental value of the $N\lambda_0$. The simulation code is provided in appendix D.

The precision result of the simulation was also shown in Fig. 5.15.

doi:10.6342/NTU202501717

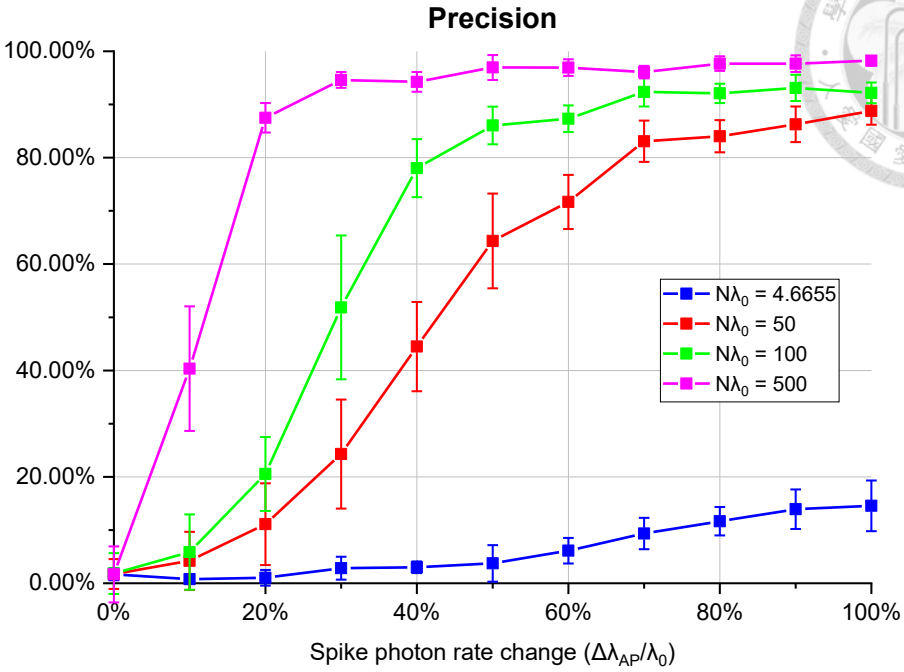

Fig. 5.15 The precision diagram of the simulation result under different $N\lambda_0$. The blue curve indicates the experimental value of the $N\lambda_0$. The simulation code is provided in appendix D.

In the result of Fig. 5.14 and Fig. 5.15, we can obviously see great promotion on either sensitivity or precision when we increased the value of $N\lambda_0$. Here for $N\lambda_0$ represents the ROI photon rate, we want to emphasize again that the quantization of the emission photon has played the most important role of the whole simulation. In conclusion, for these two parameters of $N\lambda_0$ and $\Delta\lambda_{AP}/\lambda_0$, both of them are important by getting good sensitivity or good precision of spike detection.

doi:10.6342/NTU202501717

CHAPTER 6 CONCLUSION

In this study, we have created a simulation framework to simulate a simple condition under two-photon voltage imaging photon emission from the perspective of photon statistics. For our simulation results, we can conclude that:

1. The value of $N\lambda_0$ can be the most important parameter if we want to optimize the spike detection sensitivity and precision.
2. From the perspective of microscopy system, N indicates the pixel number of region of interest (ROI) in experimental condition, which can be the most important factor to deal with.
3. From the perspective of the specimen, λ_0 and $\Delta\lambda_{AP}/\lambda_0$ represent the brightness of the specimen and the fluorescence change of the spikes, respectively, both are also important factors to optimize spike detection rate.

Here we provide some suggestions to optimize the sensitivity and precision of voltage imaging spike detection from the perspective of experimental system design:

a. To increase the number of ROI pixels, it is recommended to reduce the scanning field of view (FOV) in two-photon scanning microscopy. For example, in the experiment in 3.2, halving the FOV along the X-axis effectively halves the pixel

doi:10.6342/NTU202501717

spacing, thereby doubling the number of pixels within the same ROI area.

b. Alternatively, to increase the number of ROI pixels, reducing the frame rate in exchange for more scan lines can be considered. In our experiment, we used 10 pixels along the Y-axis, corresponding to 10 resonant scanning lines per frame. By doubling the number of scanning lines to 20, the frame rate would be halved, but the total number of pixels would be doubled.

c. To enhance the baseline image brightness, according to the photon emission number relationship described by Eq. (3.3), we recommend avoiding low numerical aperture (NA) GRIN rods or objective lenses. Instead, high-NA optics should be used. In our in vivo experiment, a GRIN rod with NA = 0.5 was used. Replacing it with an objective lens of NA = 1.0 would theoretically increase fluorescence brightness by fourfold. In addition, the average excitation power should be raised to an appropriate level, as long as photodamage to the specimen can be avoided.

Also, although we have done some calculations for our emission photon rate, which can significantly affect the spike performance quality, there is also an option to confirm if the photon rate is enough. By observing the image brightness fluctuation, due to the characteristic of quantization, the fluctuation should be stabilized while enhancing the

doi:10.6342/NTU202501717

image photon rate.

In the future, there are still some interesting extended works to do. For example, by far we have created a simulation model under perfect measurement system, how about an imperfect condition? Considering not only photon statistics but more environmental variables in the simulation, for example, the PMT pulse height distribution and the quantum efficiency.

doi:10.6342/NTU202501717

REFERENCE

[1] W. Denk, J. H. Strickler, and W. W. Webb, "Two-photon laser scanning fluorescence microscopy," *Science,* vol. 248, no. 4951, pp. 73-76, 1990.

[2] F. Helmchen and W. Denk, "Deep tissue two-photon microscopy," *Nature methods,* vol. 2, no. 12, pp. 932-940, 2005.

[3] V. Crosignani *et al.*, "Deep tissue fluorescence imaging and in vivo biological applications," *Journal of biomedical optics,* vol. 17, no. 11, pp. 116023-116023, 2012.

[4] T. Hakamata *et al.*, "Photomultiplier tubes: basics and applications," *Hamamatsu Photonics KK Electron Tube Division, Hamamatsu City,* 2006.

[5] L. Fleury, J.-M. Segura, G. Zumofen, B. Hecht, and U. Wild, "Nonclassical photon statistics in single-molecule fluorescence at room temperature," *Physical review letters,* vol. 84, no. 6, p. 1148, 2000.

[6] E. Bloemsma and J. Knoester, "Photon emission statistics and photon tracking in single-molecule spectroscopy of molecular aggregates: Dimers and trimers," *The Journal of Chemical Physics,* vol. 136, no. 22, 2012.

[7] Y. He and E. Barkai, "Super-and sub-Poissonian photon statistics for single molecule spectroscopy," *The Journal of chemical physics,* vol. 122, no. 18, 2005.

[8] W. Moerner and D. P. Fromm, "Methods of single-molecule fluorescence spectroscopy and microscopy," *Review of Scientific instruments,* vol. 74, no. 8, pp. 3597-3619, 2003.

[9] J. Schedlbauer *et al.*, "Ultrafast single-molecule fluorescence measured by femtosecond double-pulse excitation photon antibunching," *Nano Letters,* vol. 20, no. 2, pp. 1074-1079, 2019.

[10] S. M. Ross, *Introduction to probability models*. Academic press, 2014.

[11] J. Platisa and V. A. Pieribone, "Genetically encoded fluorescent voltage indicators: are we there yet?," *Current opinion in neurobiology,* vol. 50, pp. 146-153, 2018.

[12] Y. Xu, P. Zou, and A. E. Cohen, "Voltage imaging with genetically encoded indicators," *Current opinion in chemical biology,* vol. 39, pp. 1-10, 2017.

[13] A. Lab. "Voltage and calcium imaging of the same neuron." UConn Health. https://health.uconn.edu/antic-lab/image-gallery/ (accessed 6/23, 2025).

[14] S. W. Evans *et al.*, "A positively tuned voltage indicator for extended electrical recordings in the brain," *Nature Methods,* vol. 20, no. 7, pp. 1104-1113, 2023.

doi:10.6342/NTU202501717

[15] J. Platisa *et al.*, "High-speed low-light in vivo two-photon voltage imaging of large neuronal populations," *Nature methods,* vol. 20, no. 7, pp. 1095-1103, 2023.

[16] S. Zhao *et al.*, "Deep two-photon voltage imaging with adaptive excitation," *Research Square,* pp. rs. 3. rs-5434919, 2024.

[17] S. Xiao *et al.*, "Large-scale deep tissue voltage imaging with targeted-illumination confocal microscopy," *Nature methods,* vol. 21, no. 6, pp. 1094-1102, 2024.

doi:10.6342/NTU202501717

APPENDIX A 5.3.2 SIMULATION CODE

```
%% Simulated 30s Data Generation and Spike Detection
% Results with variation of photon rate (λ0)
close all; clear all;

%% ==== 全域參數設定 ====
selected_points = 1505;
bin_samples = 61538;
duration = 30.3;
fs = 80e6;
voltage_per_photon = 0.91428;
peak_amplitude = 0.2;
num_repeat = 10;

%% ==== lambda sweep 設定 ====
lambda_list = [5e4, 1e5, 2.46e5, 5e5, 1e6, 5e6, 10e6, 15e6, 20e6];
base_path = 'F:\My Drive\Main\碩士論文\Figure\Simulation result\PR';

for l_idx = 1:length(lambda_list)
    lambda_per_sec = lambda_list(l_idx);
    lambda_per_pulse = lambda_per_sec / fs;
    folder_name = sprintf('%d_%d_%d', round(lambda_per_sec),
selected_points, round(100*peak_amplitude));
    output_path = fullfile(base_path, folder_name);

    for repeat_idx = 1:num_repeat

        %% ==== 計算需用參數 ====
        num_pulses = duration * fs;
        num_bins = floor(num_pulses / bin_samples);
        bin_width_ms = 1000 * bin_samples / fs;
        bin_width_s = bin_width_ms / 1000;

        %% ==== 建立 modulation ====
```


doi:10.6342/NTU202501717

```
        t = (0:num_pulses-1) / fs;
        modulation = ones(size(t));
        peak_amplitude = 0.2;
        width = 0.5e-3;
        mod_times = 0.3:0.3:(duration-0.3);

        for k = 1:length(mod_times)
            center_time = mod_times(k);
            modulation = modulation + peak_amplitude * exp(-((t -
center_time).^2) / (2 * width^2));
        end

        lambda_modulated = lambda_per_pulse * modulation;

        %% ==== 模擬資料產生 ====
        signal_avg = zeros(1, num_bins);
        t_bin_center = zeros(1, num_bins);
        signal_matrix = poissrnd(lambda_modulated) * voltage_per_photon;

        bin_samples_first = (duration * fs / 2 - bin_samples / 2) - ...
            (floor((duration * fs / 2 - bin_samples / 2) / bin_samples)
* bin_samples);

        for i = 1:num_bins
            if i == 1
                idx_start = 1;
                idx_end = selected_points;
                idx_end_t = idx_start + bin_samples_first - 1;
            elseif i == num_bins
                idx_start = bin_samples_first + (i - 2) * bin_samples +
1;
                idx_end = idx_start + selected_points;
                idx_end_t = idx_start + bin_samples_first;
            else
                idx_start = bin_samples_first + (i - 2) * bin_samples +
1;
```


doi:10.6342/NTU202501717

```
            idx_end = idx_start + selected_points - 1;
            idx_end_t = idx_start + bin_samples - 1;
        end
        if idx_end > num_pulses, break; end
        t_bin_center(i) = mean((idx_start:idx_end_t) / fs);
        signal_avg(i) = mean(signal_matrix(idx_start:idx_end));
    end

    %% ==== Spike Detection Method ====
    delta_bin_ms = 1;
    bins_dt = round(delta_bin_ms / bin_width_ms);
    bin_window_1s = round(1 / bin_width_s);
    bin_window_01s = round(0.1 / bin_width_s);
    baseline_window = round(0.4 / bin_width_s);
    F_baseline = movmean(signal_avg, baseline_window,
'Endpoints','shrink');
    F_dr = min(signal_avg, F_baseline);
    F_ur = max(signal_avg, F_baseline);

    F_dr_shift = [F_dr(1)*ones(1,bins_dt), F_dr(1:end-bins_dt)];
    F_ur_shift = [F_ur(1)*ones(1,bins_dt), F_ur(1:end-bins_dt)];
    dF_dr = F_dr - F_dr_shift;
    dF_ur = F_ur - F_ur_shift;

    spike_mark = zeros(size(signal_avg));
    spike_color = zeros(size(signal_avg));
    mod_idx = [];
    for mt = mod_times
        mod_idx = [mod_idx, find(abs(t_bin_center - mt) <= 0.001)];
    end

    for i = 2:length(signal_avg)
        idx_range_1s = max(1, i-
bin_window_1s):min(length(signal_avg), i+bin_window_1s);
        idx_range_01s = max(1, i-
bin_window_01s):min(length(signal_avg), i+bin_window_01s);
```


doi:10.6342/NTU202501717

```
            mean_dF_ur_local = mean(dF_ur(idx_range_1s));
            std_dF_dr_local = std(dF_dr(idx_range_1s));
            mean_signal_local = mean(signal_avg(idx_range_01s));
            sigma_F_local = 2 * std(F_dr(idx_range_1s));

            bins_3ms = round(3 / bin_width_ms);
            if i > bins_3ms
                F_AP = max(signal_avg(i) - signal_avg(i-bins_3ms:i));
            else
                F_AP = 0;
            end

            cond1 = dF_ur(i) > mean_dF_ur_local + 3 * std_dF_dr_local;
            cond2 = signal_avg(i) > mean_signal_local + 3 *
sigma_F_local;
            cond3 = F_AP > 4 * sigma_F_local;

            if cond1 && cond2 && cond3
                spike_mark(i) = 1;
                if ismember(i, mod_idx)
                    spike_color(i) = 1;
                end
            end
        end

        %% ==== 每個 modulation 區間只保留一個 ====
        filtered_spike_mark = zeros(size(spike_mark));
        filtered_spike_color = zeros(size(spike_color));

        for mt = mod_times
            idx_range = find(abs(t_bin_center - mt) <= 0.001);
            spike_in_range = idx_range(spike_mark(idx_range) == 1 &
spike_color(idx_range) == 1);
            if ~isempty(spike_in_range)
                [~, max_idx] = max(signal_avg(spike_in_range));
```


doi:10.6342/NTU202501717

```
            keep_idx = spike_in_range(max_idx);
            filtered_spike_mark(keep_idx) = 1;
            filtered_spike_color(keep_idx) = 1;
        end
    end

    % spike 標記
    spike_mark = (spike_mark == 1 & spike_color == 0);
    spike_mark = spike_mark + filtered_spike_mark;
    spike_color = filtered_spike_color;

    %% ==== 統計與畫圖 ====
    positive_count = sum(spike_mark);
    TP = sum(spike_color);
    FP = positive_count - TP;
    [u,spike_num] = size(mod_times);
    FN = spike_num - TP;

    positive_rate = positive_count / duration;

    figure('Position', [100, 100, 1400, 600]);
    plot(t_bin_center, signal_avg); hold on;

    % modulation 垂直線
    for mt = mod_times
        xline(mt, '--g', 'LineWidth', 1);
    end

    % 畫 spike 點
    plot(t_bin_center(spike_mark==1 & spike_color==0),
signal_avg(spike_mark==1 & spike_color==0), 'ro', ...
        'MarkerFaceColor','r', 'MarkerSize',5);
    plot(t_bin_center(spike_mark==1 & spike_color==1),
signal_avg(spike_mark==1 & spike_color==1), 'go', ...
        'MarkerFaceColor','g', 'MarkerSize',5);
```


doi:10.6342/NTU202501717

```
        xlabel('Time (s)');
        ylabel('Voltage(V)');

        title_str = sprintf(('%ds , $\\lambda$ = %.4f / pulse , Bin = %d
pts , spike amplitude %d\\%%\n%d spikes added / %d spikes detected (%d
TP / %d FP / %d FN)\n Precision($ \\frac{TP}{TP + FP}$) = %.1f\\%% /
Sensitivity($ \\frac{TP}{TP + FN}$) = %.1f\\%%'),...
            duration, lambda_per_pulse,selected_points,round(100 *
peak_amplitude),spike_num, positive_count, TP, FP, FN, 100*TP/(TP+FP),
100*TP/(TP+FN));

        title(title_str, 'Interpreter', 'latex');
        grid on;

        filename = sprintf('%d.png', repeat_idx);
        saveas(gcf, fullfile(output_path, filename));
        close(gcf);
        clear signal_matrix modulation lambda_modulated F_baseline F_dr
F_ur ...
         F_dr_shift F_ur_shift dF_dr dF_ur signal_avg t t_bin_center
    end
end
```


doi:10.6342/NTU202501717

APPENDIX B 5.3.3 SIMULATION CODE

```
%% Simulated 30s Data Generation and Spike Detection
% Results with variation of bin number (N)
close all; clear all;

%% ==== 全域參數設定 ====
bin_samples = 61538;
duration = 30.3;
fs = 80e6;
voltage_per_photon = 0.91428;
lambda_per_sec = 2.46e5;
peak_amplitude = 0.2;
num_repeat = 10;

%% ==== N sweep 設定 ====
selected_points_list = [200, 500, 1000, 1505, 5000, 10000, 15000,
20000, 25000, 30000, 35000, 40000, 45000, 50000, 50000];
base_path = 'F:\My Drive\Main\碩士論文\Figure\Simulation result\BN';

for l_idx = 1:length(selected_points_list)
    selected_points = selected_points_list(l_idx);
    lambda_per_pulse = lambda_per_sec / fs;
    folder_name = sprintf('%d_%d_%d', round(lambda_per_sec),
selected_points, round(100*peak_amplitude));
    output_path = fullfile(base_path, folder_name);

    for repeat_idx = 1:num_repeat

        %% ==== 計算需用參數 ====
        num_pulses = duration * fs;
        num_bins = floor(num_pulses / bin_samples);
        bin_width_ms = 1000 * bin_samples / fs;
        bin_width_s = bin_width_ms / 1000;

        %% ==== 建立 modulation ====
```


doi:10.6342/NTU202501717

```
        t = (0:num_pulses-1) / fs;
        modulation = ones(size(t));
        peak_amplitude = 0.2;
        width = 0.5e-3;  % 0.5 ms
        mod_times = 0.3:0.3:(duration-0.3);

        for k = 1:length(mod_times)
            center_time = mod_times(k);
            modulation = modulation + peak_amplitude * exp(-((t -
center_time).^2) / (2 * width^2));
        end

        lambda_modulated = lambda_per_pulse * modulation;

        %% ==== 模擬資料產生 ====
        signal_avg = zeros(1, num_bins);
        t_bin_center = zeros(1, num_bins);
        signal_matrix = poissrnd(lambda_modulated) * voltage_per_photon;

        bin_samples_first = (duration * fs / 2 - bin_samples / 2) - ...
            (floor((duration * fs / 2 - bin_samples / 2) / bin_samples)
* bin_samples);

        for i = 1:num_bins
            if i == 1
                idx_start = 1;
                idx_end = selected_points;
                idx_end_t = idx_start + bin_samples_first - 1;
            elseif i == num_bins
                idx_start = bin_samples_first + (i - 2) * bin_samples +
1;
                idx_end = idx_start + selected_points;
                idx_end_t = idx_start + bin_samples_first;
            else
                idx_start = bin_samples_first + (i - 2) * bin_samples +
1;
```


doi:10.6342/NTU202501717

```
            idx_end = idx_start + selected_points - 1;
            idx_end_t = idx_start + bin_samples - 1;
        end
        if idx_end > num_pulses, break; end
        t_bin_center(i) = mean((idx_start:idx_end_t) / fs);
        signal_avg(i) = mean(signal_matrix(idx_start:idx_end));
    end

    %% ==== Spike Detection Method ====
    delta_bin_ms = 1;
    bins_dt = round(delta_bin_ms / bin_width_ms);
    bin_window_1s = round(1 / bin_width_s);
    bin_window_01s = round(0.1 / bin_width_s);
    baseline_window = round(0.4 / bin_width_s);
    F_baseline = movmean(signal_avg, baseline_window,
'Endpoints','shrink');
    F_dr = min(signal_avg, F_baseline);
    F_ur = max(signal_avg, F_baseline);

    F_dr_shift = [F_dr(1)*ones(1,bins_dt), F_dr(1:end-bins_dt)];
    F_ur_shift = [F_ur(1)*ones(1,bins_dt), F_ur(1:end-bins_dt)];
    dF_dr = F_dr - F_dr_shift;
    dF_ur = F_ur - F_ur_shift;

    spike_mark = zeros(size(signal_avg));
    spike_color = zeros(size(signal_avg));
    mod_idx = [];
    for mt = mod_times
        mod_idx = [mod_idx, find(abs(t_bin_center - mt) <= 0.001)];
    end

    for i = 2:length(signal_avg)
        idx_range_1s = max(1, i-
bin_window_1s):min(length(signal_avg), i+bin_window_1s);
        idx_range_01s = max(1, i-
bin_window_01s):min(length(signal_avg), i+bin_window_01s);
```


doi:10.6342/NTU202501717

```
            mean_dF_ur_local = mean(dF_ur(idx_range_1s));
            std_dF_dr_local = std(dF_dr(idx_range_1s));
            mean_signal_local = mean(signal_avg(idx_range_01s));
            sigma_F_local = 2 * std(F_dr(idx_range_1s));

            bins_3ms = round(3 / bin_width_ms);
            if i > bins_3ms
                F_AP = max(signal_avg(i) - signal_avg(i-bins_3ms:i));
            else
                F_AP = 0;
            end

            cond1 = dF_ur(i) > mean_dF_ur_local + 3 * std_dF_dr_local;
            cond2 = signal_avg(i) > mean_signal_local + 3 *
sigma_F_local;
            cond3 = F_AP > 4 * sigma_F_local;

            if cond1 && cond2 && cond3
                spike_mark(i) = 1;
                if ismember(i, mod_idx)
                    spike_color(i) = 1;
                end
            end
        end

        filtered_spike_mark = zeros(size(spike_mark));
        filtered_spike_color = zeros(size(spike_color));

        for mt = mod_times
            idx_range = find(abs(t_bin_center - mt) <= 0.001);
            spike_in_range = idx_range(spike_mark(idx_range) == 1 &
spike_color(idx_range) == 1);
            if ~isempty(spike_in_range)
                [~, max_idx] = max(signal_avg(spike_in_range));
                keep_idx = spike_in_range(max_idx);
```


doi:10.6342/NTU202501717

```
            filtered_spike_mark(keep_idx) = 1;
            filtered_spike_color(keep_idx) = 1;
        end
    end

    % spike 標記
    spike_mark = (spike_mark == 1 & spike_color == 0);
    spike_mark = spike_mark + filtered_spike_mark;
    spike_color = filtered_spike_color;

    %% ==== 統計與畫圖 ====
    positive_count = sum(spike_mark);
    TP = sum(spike_color);
    FP = positive_count - TP;
    [u,spike_num] = size(mod_times);
    FN = spike_num - TP;

    positive_rate = positive_count / duration;

    figure('Position', [100, 100, 1400, 600]);
    plot(t_bin_center, signal_avg); hold on;

    % modulation 垂直線
    for mt = mod_times
        xline(mt, '--g', 'LineWidth', 1);
    end

    % 畫 spike 點
    plot(t_bin_center(spike_mark==1 & spike_color==0),
signal_avg(spike_mark==1 & spike_color==0), 'ro', ...
        'MarkerFaceColor','r', 'MarkerSize',5);  % FP
    plot(t_bin_center(spike_mark==1 & spike_color==1),
signal_avg(spike_mark==1 & spike_color==1), 'go', ...
        'MarkerFaceColor','g', 'MarkerSize',5);  % TP

    xlabel('Time (s)');
```


doi:10.6342/NTU202501717

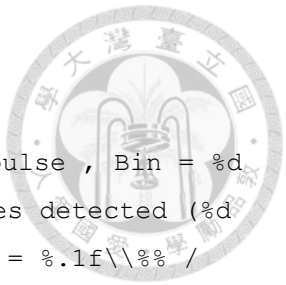

```
        ylabel('Voltage(V)');

        title_str = sprintf(('%ds , $\\lambda$ = %.4f / pulse , Bin = %d
pts , spike amplitude %d\\%%\n%d spikes added / %d spikes detected (%d
TP / %d FP / %d FN)\n Precision($ \\frac{TP}{TP + FP}$) = %.1f\\%% /
Sensitivity($ \\frac{TP}{TP + FN}$) = %.1f\\%%'),...
            duration, lambda_per_pulse,selected_points,round(100 *
peak_amplitude),spike_num, positive_count, TP, FP, FN, 100*TP/(TP+FP),
100*TP/(TP+FN));

        title(title_str, 'Interpreter', 'latex');
        grid on;

        filename = sprintf('%d.png', repeat_idx);
        saveas(gcf, fullfile(output_path, filename));
        close(gcf);
        clear signal_matrix modulation lambda_modulated F_baseline F_dr
F_ur ...
         F_dr_shift F_ur_shift dF_dr dF_ur signal_avg t t_bin_center
    end
end
```


doi:10.6342/NTU202501717

APPENDIX C 5.3.4 SIMULATION CODE

```
%% Simulated 30s Data Generation and Spike Detection
% Results with variation of spike photon rate change (ΔλAP/λ0)
close all; clear all;

%% ==== 全域參數設定 ====
selected_points = 1505;
bin_samples = 61538;
duration = 30.3;
fs = 80e6;
voltage_per_photon = 0.91428;
lambda_per_sec = 2.46e5;
num_repeat = 10;

%% ==== peak_amplitude 設定 ====
peak_amplitude_list = 0:0.1:1.2;
base_path = 'F:\My Drive\Main\碩士論文\Figure\Simulation result\FC';

for l_idx = 1:length(peak_amplitude_list)
    peak_amplitude = peak_amplitude_list(l_idx);
    lambda_per_pulse = lambda_per_sec / fs;
    folder_name = sprintf('%d_%d_%d', round(lambda_per_sec),
selected_points, round(100*peak_amplitude));
    output_path = fullfile(base_path, folder_name);

    for repeat_idx = 1:num_repeat

        %% ==== 計算需用參數 ====
        num_pulses = duration * fs;
        num_bins = floor(num_pulses / bin_samples);
        bin_width_ms = 1000 * bin_samples / fs;
        bin_width_s = bin_width_ms / 1000;

        %% ==== 建立 modulation ====
        t = (0:num_pulses-1) / fs;
```


doi:10.6342/NTU202501717

```
        modulation = ones(size(t));
        width = 0.5e-3;
        mod_times = 0.3:0.3:(duration-0.3);

        for k = 1:length(mod_times)
            center_time = mod_times(k);
            modulation = modulation + peak_amplitude * exp(-((t -
center_time).^2) / (2 * width^2));
        end

        lambda_modulated = lambda_per_pulse * modulation;

        %% ==== 模擬資料產生 ====
        signal_avg = zeros(1, num_bins);
        t_bin_center = zeros(1, num_bins);
        signal_matrix = poissrnd(lambda_modulated) * voltage_per_photon;

        bin_samples_first = (duration * fs / 2 - bin_samples / 2) - ...
            (floor((duration * fs / 2 - bin_samples / 2) / bin_samples)
* bin_samples);

        for i = 1:num_bins
            if i == 1
                idx_start = 1;
                idx_end = selected_points;
                idx_end_t = idx_start + bin_samples_first - 1;
            elseif i == num_bins
                idx_start = bin_samples_first + (i - 2) * bin_samples +
1;
                idx_end = idx_start + selected_points;
                idx_end_t = idx_start + bin_samples_first;
            else
                idx_start = bin_samples_first + (i - 2) * bin_samples +
1;
                idx_end = idx_start + selected_points - 1;
                idx_end_t = idx_start + bin_samples - 1;
```


doi:10.6342/NTU202501717

```
            end
            if idx_end > num_pulses, break; end
            t_bin_center(i) = mean((idx_start:idx_end_t) / fs);
            signal_avg(i) = mean(signal_matrix(idx_start:idx_end));
        end

        %% ==== Spike Detection Method ====
        delta_bin_ms = 1;
        bins_dt = round(delta_bin_ms / bin_width_ms);
        bin_window_1s = round(1 / bin_width_s);
        bin_window_01s = round(0.1 / bin_width_s);
        baseline_window = round(0.4 / bin_width_s);
        F_baseline = movmean(signal_avg, baseline_window,
'Endpoints','shrink');
        F_dr = min(signal_avg, F_baseline);
        F_ur = max(signal_avg, F_baseline);

        F_dr_shift = [F_dr(1)*ones(1,bins_dt), F_dr(1:end-bins_dt)];
        F_ur_shift = [F_ur(1)*ones(1,bins_dt), F_ur(1:end-bins_dt)];
        dF_dr = F_dr - F_dr_shift;
        dF_ur = F_ur - F_ur_shift;

        spike_mark = zeros(size(signal_avg));
        spike_color = zeros(size(signal_avg));
        mod_idx = [];
        for mt = mod_times
            mod_idx = [mod_idx, find(abs(t_bin_center - mt) <= 0.001)];
        end

        for i = 2:length(signal_avg)
            idx_range_1s = max(1, i-
bin_window_1s):min(length(signal_avg), i+bin_window_1s);
            idx_range_01s = max(1, i-
bin_window_01s):min(length(signal_avg), i+bin_window_01s);

            mean_dF_ur_local = mean(dF_ur(idx_range_1s));
```


doi:10.6342/NTU202501717

```
            std_dF_dr_local = std(dF_dr(idx_range_1s));
            mean_signal_local = mean(signal_avg(idx_range_01s));
            sigma_F_local = 2 * std(F_dr(idx_range_1s));

            bins_3ms = round(3 / bin_width_ms);
            if i > bins_3ms
                F_AP = max(signal_avg(i) - signal_avg(i-bins_3ms:i));
            else
                F_AP = 0;
            end

            cond1 = dF_ur(i) > mean_dF_ur_local + 3 * std_dF_dr_local;
            cond2 = signal_avg(i) > mean_signal_local + 3 *
sigma_F_local;
            cond3 = F_AP > 4 * sigma_F_local;

            if cond1 && cond2 && cond3
                spike_mark(i) = 1;
                if ismember(i, mod_idx)
                    spike_color(i) = 1;
                end
            end
        end

        %% ==== 每個 modulation 區間只保留一個 TP（最大值） ====
        filtered_spike_mark = zeros(size(spike_mark));
        filtered_spike_color = zeros(size(spike_color));

        for mt = mod_times
            idx_range = find(abs(t_bin_center - mt) <= 0.001);
            spike_in_range = idx_range(spike_mark(idx_range) == 1 &
spike_color(idx_range) == 1);
            if ~isempty(spike_in_range)
                [~, max_idx] = max(signal_avg(spike_in_range));
                keep_idx = spike_in_range(max_idx);
                filtered_spike_mark(keep_idx) = 1;
```


doi:10.6342/NTU202501717

```
            filtered_spike_color(keep_idx) = 1;
        end
    end

    % spike 標記
    spike_mark = (spike_mark == 1 & spike_color == 0);
    spike_mark = spike_mark + filtered_spike_mark;
    spike_color = filtered_spike_color;

    %% ==== 統計與畫圖 ====
    positive_count = sum(spike_mark);
    TP = sum(spike_color);
    FP = positive_count - TP;
    [u,spike_num] = size(mod_times);
    FN = spike_num - TP;

    positive_rate = positive_count / duration;

    figure('Position', [100, 100, 1400, 600]);
    plot(t_bin_center, signal_avg); hold on;

    % modulation 垂直線
    for mt = mod_times
        xline(mt, '--g', 'LineWidth', 1);
    end

    % 畫 spike 點
    plot(t_bin_center(spike_mark==1 & spike_color==0),
signal_avg(spike_mark==1 & spike_color==0), 'ro', ...
        'MarkerFaceColor','r', 'MarkerSize',5);
    plot(t_bin_center(spike_mark==1 & spike_color==1),
signal_avg(spike_mark==1 & spike_color==1), 'go', ...
        'MarkerFaceColor','g', 'MarkerSize',5);

    xlabel('Time (s)');
    ylabel('Voltage(V)');
```


doi:10.6342/NTU202501717

```
      title_str = sprintf(('%ds , $\\lambda$ = %.4f / pulse , Bin = %d
pts , spike amplitude %d\\%%\n%d spikes added / %d spikes detected (%d
TP / %d FP / %d FN)\n Precision($ \\frac{TP}{TP + FP}$) = %.1f\\%% /
Sensitivity($ \\frac{TP}{TP + FN}$) = %.1f\\%%'),...
          duration, lambda_per_pulse,selected_points,round(100 *
peak_amplitude),spike_num, positive_count, TP, FP, FN, 100*TP/(TP+FP),
100*TP/(TP+FN));

      title(title_str, 'Interpreter', 'latex');
      grid on;

      filename = sprintf('%d.png', repeat_idx);
      saveas(gcf, fullfile(output_path, filename));
      close(gcf);
      clear signal_matrix modulation lambda_modulated F_baseline F_dr
F_ur ...
       F_dr_shift F_ur_shift dF_dr dF_ur signal_avg t t_bin_center
   end
end
```


doi:10.6342/NTU202501717

APPENDIX D 5.5 SIMULATION CODE

```
%% Simulated 30s Data Generation and Spike Detection
% 5.14 5.15 simulation code
% Results with variation NΛ0
close all; clear all;

%% ==== 全域參數設定 ====
selected_points = 1505;
bin_samples = 61538;
duration = 30.3;
fs = 80e6;
voltage_per_photon = 0.91428;
N_lambda = 10;
lambda_per_sec = (N_lambda/selected_points)*fs;
num_repeat = 10;

%% ==== peak_amplitude 設定 ====
peak_amplitude_list = 0:0.1:1.0;
base_path = 'F:\My Drive\Main\碩士論文\Figure\Simulation
result\BNPR\10';

for l_idx = 1:length(peak_amplitude_list)
    peak_amplitude = peak_amplitude_list(l_idx);
    lambda_per_pulse = lambda_per_sec / fs;
    folder_name = sprintf('%d', round(100*peak_amplitude));
    output_path = fullfile(base_path, folder_name);

    for repeat_idx = 1:num_repeat

        %% ==== 計算需用參數 ====
        num_pulses = duration * fs;
        num_bins = floor(num_pulses / bin_samples);
        bin_width_ms = 1000 * bin_samples / fs;
        bin_width_s = bin_width_ms / 1000;
```


doi:10.6342/NTU202501717

```
%% ==== 建立 modulation ====
t = (0:num_pulses-1) / fs;
modulation = ones(size(t));
width = 0.5e-3;  % 0.5 ms
mod_times = 0.3:0.3:(duration-0.3);

for k = 1:length(mod_times)
    center_time = mod_times(k);
    modulation = modulation + peak_amplitude * exp(-((t -
center_time).^2) / (2 * width^2));
end

lambda_modulated = lambda_per_pulse * modulation;

%% ==== 模擬資料產生 ====
signal_avg = zeros(1, num_bins);
t_bin_center = zeros(1, num_bins);
signal_matrix = poissrnd(lambda_modulated) * voltage_per_photon;

bin_samples_first = (duration * fs / 2 - bin_samples / 2) - ...
    (floor((duration * fs / 2 - bin_samples / 2) / bin_samples)
* bin_samples);

for i = 1:num_bins
    if i == 1
        idx_start = 1;
        idx_end = selected_points;
        idx_end_t = idx_start + bin_samples_first - 1;
    elseif i == num_bins
        idx_start = bin_samples_first + (i - 2) * bin_samples +
1;
        idx_end = idx_start + selected_points;
        idx_end_t = idx_start + bin_samples_first;
    else
        idx_start = bin_samples_first + (i - 2) * bin_samples +
1;
```


doi:10.6342/NTU202501717

```
            idx_end = idx_start + selected_points - 1;
            idx_end_t = idx_start + bin_samples - 1;
        end
        if idx_end > num_pulses, break; end
        t_bin_center(i) = mean((idx_start:idx_end_t) / fs);  % 單位是
秒（s）
        signal_avg(i) = mean(signal_matrix(idx_start:idx_end));
    end

    %% ==== Spike Detection Method ====
    delta_bin_ms = 1;
    bins_dt = round(delta_bin_ms / bin_width_ms);
    bin_window_1s = round(1 / bin_width_s);
    bin_window_01s = round(0.1 / bin_width_s);
    baseline_window = round(0.4 / bin_width_s);
    F_baseline = movmean(signal_avg, baseline_window,
'Endpoints','shrink');
    F_dr = min(signal_avg, F_baseline);
    F_ur = max(signal_avg, F_baseline);

    F_dr_shift = [F_dr(1)*ones(1,bins_dt), F_dr(1:end-bins_dt)];
    F_ur_shift = [F_ur(1)*ones(1,bins_dt), F_ur(1:end-bins_dt)];
    dF_dr = F_dr - F_dr_shift;
    dF_ur = F_ur - F_ur_shift;

    spike_mark = zeros(size(signal_avg));
    spike_color = zeros(size(signal_avg));
    mod_idx = [];
    for mt = mod_times
        mod_idx = [mod_idx, find(abs(t_bin_center - mt) <= 0.001)];
    end

    for i = 2:length(signal_avg)
        idx_range_1s = max(1, i-
bin_window_1s):min(length(signal_avg), i+bin_window_1s);
        idx_range_01s = max(1, i-
```


doi:10.6342/NTU202501717

```
bin_window_01s):min(length(signal_avg), i+bin_window_01s);

          mean_dF_ur_local = mean(dF_ur(idx_range_1s));
          std_dF_dr_local = std(dF_dr(idx_range_1s));
          mean_signal_local = mean(signal_avg(idx_range_01s));
          sigma_F_local = 2 * std(F_dr(idx_range_1s));

          bins_3ms = round(3 / bin_width_ms);
          if i > bins_3ms
             F_AP = max(signal_avg(i) - signal_avg(i-bins_3ms:i));
          else
             F_AP = 0;
          end

          cond1 = dF_ur(i) > mean_dF_ur_local + 3 * std_dF_dr_local;
          cond2 = signal_avg(i) > mean_signal_local + 3 *
sigma_F_local;
          cond3 = F_AP > 4 * sigma_F_local;

          if cond1 && cond2 && cond3
             spike_mark(i) = 1;
             if ismember(i, mod_idx)
                spike_color(i) = 1;
             end
          end
       end

       %% ==== 每個 modulation 區間只保留一個 TP ====
       filtered_spike_mark = zeros(size(spike_mark));
       filtered_spike_color = zeros(size(spike_color));

       for mt = mod_times
          idx_range = find(abs(t_bin_center - mt) <= 0.001);
          spike_in_range = idx_range(spike_mark(idx_range) == 1 &
spike_color(idx_range) == 1);
          if ~isempty(spike_in_range)
```


doi:10.6342/NTU202501717

```
            [~, max_idx] = max(signal_avg(spike_in_range));
            keep_idx = spike_in_range(max_idx);
            filtered_spike_mark(keep_idx) = 1;
            filtered_spike_color(keep_idx) = 1;
        end
    end

    % spike 標記
    spike_mark = (spike_mark == 1 & spike_color == 0);
    spike_mark = spike_mark + filtered_spike_mark;
    spike_color = filtered_spike_color;

    %% ==== 統計與畫圖 ====
    positive_count = sum(spike_mark);
    TP = sum(spike_color);
    FP = positive_count - TP;
    [u,spike_num] = size(mod_times);
    FN = spike_num - TP;

    positive_rate = positive_count / duration;

    figure('Position', [100, 100, 1400, 600]);
    plot(t_bin_center, signal_avg); hold on;

    % modulation 垂直線
    for mt = mod_times
        xline(mt, '--g', 'LineWidth', 1);
    end

    % 畫 spike 點
    plot(t_bin_center(spike_mark==1 & spike_color==0),
signal_avg(spike_mark==1 & spike_color==0), 'ro', ...
        'MarkerFaceColor','r', 'MarkerSize',5);
    plot(t_bin_center(spike_mark==1 & spike_color==1),
signal_avg(spike_mark==1 & spike_color==1), 'go', ...
        'MarkerFaceColor','g', 'MarkerSize',5);
```


doi:10.6342/NTU202501717

```
        xlabel('Time (s)');
        ylabel('Voltage(V)');

        title_str = sprintf(('%ds , N$\\lambda$ = %.2f , spike amplitude
%d\\%%\n%d spikes added / %d spikes detected (%d TP / %d FP / %d FN)\n
Precision($ \\frac{TP}{TP + FP}$) = %.1f\\%% / Sensitivity($
\\frac{TP}{TP + FN}$) = %.1f\\%%'),...
            duration, N_lambda, round(100 * peak_amplitude),spike_num,
positive_count, TP, FP, FN, 100*TP/(TP+FP), 100*TP/(TP+FN));

        title(title_str, 'Interpreter', 'latex');
        grid on;

        filename = sprintf('%d.png', repeat_idx);
        saveas(gcf, fullfile(output_path, filename));
        close(gcf);
        clear signal_matrix modulation lambda_modulated F_baseline F_dr
F_ur ...
         F_dr_shift F_ur_shift dF_dr dF_ur signal_avg t t_bin_center
    end
end
```


doi:10.6342/NTU202501717